

# Thermal evolution of the Sierra Nevada batholith, California, and implications for strain localization

Elisabeth S. Nadin<sup>1</sup>, Jason Saleeby<sup>2</sup>, and Martin Wong<sup>3</sup>

<sup>1</sup>Department of Geosciences, University of Alaska Fairbanks, Fairbanks, Alaska 99775-5780, USA

<sup>2</sup>Division of Geological and Planetary Sciences, California Institute of Technology, MS 100-23, Pasadena, California 91125, USA

<sup>3</sup>Department of Geology, 428 Ho Science Center, Colgate University, 13 Oak Drive, Hamilton, New York 13346, USA

## ABSTRACT

The Sierra Nevada batholith (California, USA) hosts multiple shear zones of different ages and different styles of deformation. In this study we present new data syntheses and maps of U-Pb zircon and hornblende and biotite Ar age distributions through the batholith in order to examine the temporal and thermal settings under which contractional and transpressional shear zones arose. These maps highlight the localization of intrabatholithic shear zones at the boundaries between swaths of some of the oldest and youngest plutons, and help to distinguish deformation styles in the southern and central Sierran arc. We also present new <sup>40</sup>Ar/<sup>39</sup>Ar ages and crystallization and deformation temperatures from along the Kern Canyon fault system in the southern part of the batholith, and contrast these new constraints with previously published thermochronological conditions for shear zones to the north. The transpressional proto-Kern Canyon fault was continuously active from ca. 95 to 85 Ma. Deformation temperatures along the fault increase by ~100 °C from north to south, following the trend of increasing pluton emplacement pressures. These observations, in conjunction with a steep cooling path for the southeastern section of the batholith east of the proto-Kern Canyon fault, support previous interpretations that rapid exhumation in the southernmost part of the batholith followed the arrival and low-angle subduction of an oceanic plateau (the Shatsky Rise conjugate). We suggest that local forces such as these triggered mid-Cretaceous shear zone development in the southern Sierra Nevada batholith, while shear zones in the central part of the batholith, which record the transition from 100–90 Ma compression to 90–80 Ma transpression, were triggered by changing kinematic patterns in regional subduction forcing. This idea is supported by our thermochronologic color contour maps, which reveal an east-west-trending older (and colder) swath within the batholith that may have prevented the more northern shear zones from propagating southward. We contrast the cooling paths of regions within the southernmost part of the batholith, and propose a two-part deformation history in which (1) the 95–85 Ma ductile proto-Kern Canyon fault initiated in the southeast as a compressional structure that transitioned to transpressional, and (2) the 85–75(?) Ma ductile to brittle Kern Canyon–White Wolf fault initiated in the southwest, accommodated extrusion of shallowly subducted accretionary material and thinning of the overlying batholith, and then overprinted the proto-Kern Can-

yon fault along its northern end. Shear zone activity within the central Sierra Nevada batholith can thus be distinguished by location: in the central zone deformation arose from regional forces, and in the southern zone deformation was triggered by local forces.

## INTRODUCTION

Continental arcs preserve complex deformation histories imparted by subduction zone–forced normal and tangential stresses. In the Cretaceous arc of the central and southern Sierra Nevada (California, USA), intra-arc deformation is recorded by 14 mapped discrete ductile and ductile-brittle shear zones (Fig. 1) that are preserved at plutonic levels of the arc. Many of the shear zones in the central part of the Sierra Nevada batholith (SNB) have been well studied in terms of timing, sense of motion, pressure and temperature conditions during deformation, and rock fabrics. Deformation conditions and timing of major shear zone deformation in the southernmost part of the batholith, however, have been constrained mainly via the regional context of pluton emplacement and cooling (Saleeby and Busby-Spera, 1986; Busby-Spera and Saleeby, 1990; Nadin and Saleeby, 2008). The Kern Canyon system in the south (Fig. 1) appears to have a more complex polyphase history than shear zones of the central Sierran arc. Here we present new <sup>40</sup>Ar/<sup>39</sup>Ar ages and plagioclase-hornblende, two-plagioclase, and Ti-in-quartz thermometry in order to constrain the timing and thermal conditions of deformation along the proto-Kern Canyon fault. We present a model wherein the proto-Kern Canyon fault arose independently from its northern neighbors, and is distinguished from the kinematic history of the Kern Canyon–White Wolf fault.

In addition, we summarize all published U-Pb zircon, K-Ar, and <sup>40</sup>Ar/<sup>39</sup>Ar hornblende and biotite ages, and create age-distribution maps from each of these data sets in order to track regional-scale batholithic cooling from temperatures of crystallization (U-Pb zircon) through the transition to brittle conditions (Ar biotite). Despite widespread sampling throughout the batholith, from which arose studies focusing on regional patterns in crystallization depths (Ague and Brimhall, 1988; Pickett and Saleeby, 1993; Dixon, 1995; Ague, 1997; Brady et al., 2006; Nadin and Saleeby, 2008; Chapman et al., 2012), there have not yet been any comprehensive syntheses of its thermal evolution.

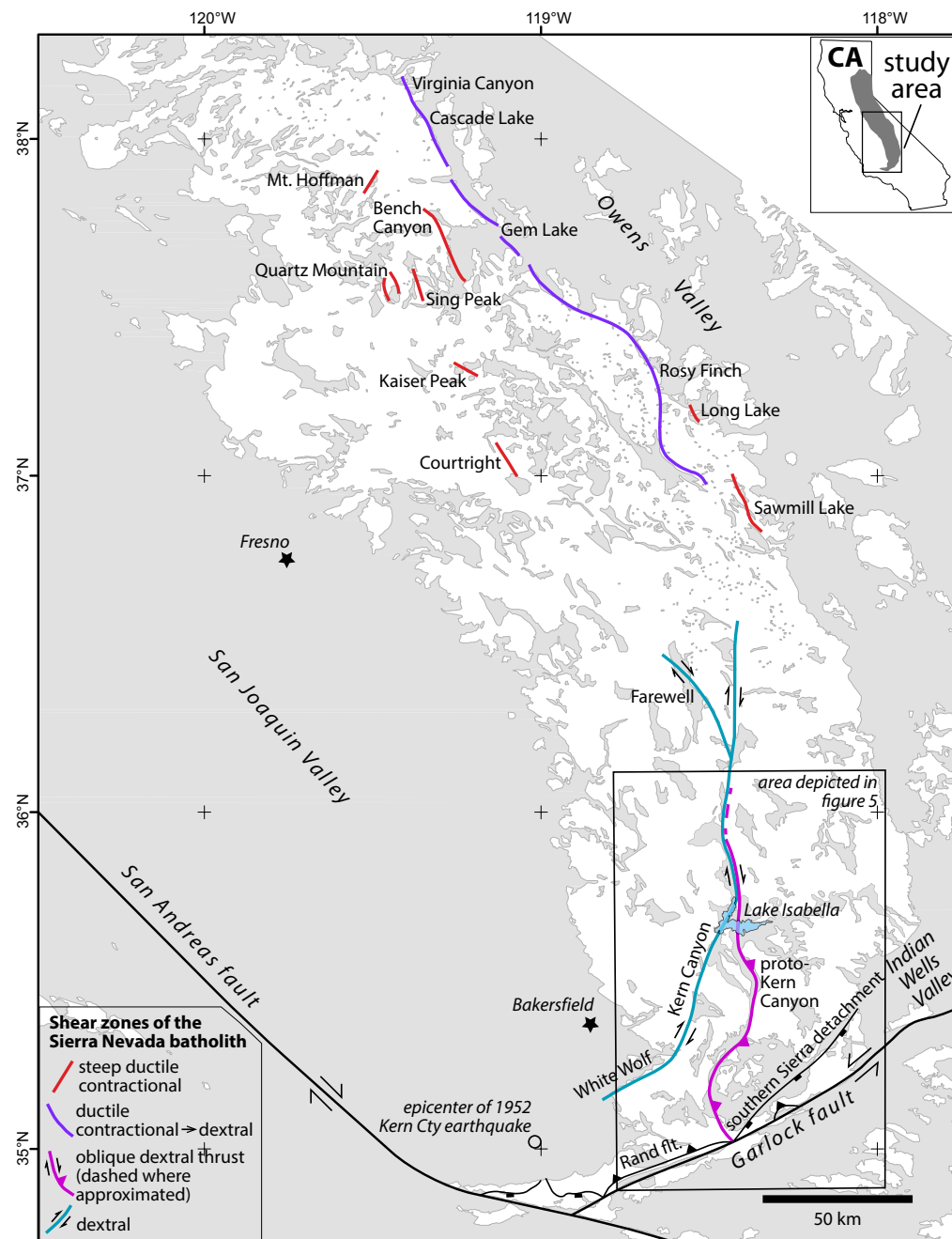


Figure 1. Overview map of the Sierra Nevada batholith, with major geographic features for orientation. Inset map shows the outline of the batholith in California (CA); white represents plutonic exposures, and gray indicates metamorphic and volcanic pendants. The 14 shear zones of the batholith are discussed in the text (excluding the Farewell fault, which lacks age control), and are differentiated by age and type of deformation as depicted by the different colors shown here. The proto-Kern Canyon fault roots into the Rand fault, and the Kern Canyon–White Wolf fault is related to the southern Sierra detachment system (see text).

Regional-scale thermal modeling of the SNB (Barton and Hanson, 1989) that is particularly well posed for assessing the temporal, spatial, and volumetric patterns in the central to southern batholith reveals that, despite large magma fluxes over time, strong horizontal thermal gradients developed between longitudinal age zones of the batholith. Such circumstances are ideal for strain localization, which is a major focus of our observational data-based analysis. Given the important role of temperature in localizing deformation, we examine in detail the thermal conditions under which the major shear zones were active, with focus on the southern part of the batholith and the proto-Kern Canyon fault, along which there is a significant range in exposure depths. The region has been mapped at various scales (Saleeby and Busby-Spera, 1986; Wood and Saleeby, 1997; Saleeby et al., 2008), and the early shortening history of the fault has been described (Nadin and Saleeby, 2008). We seek here to further constrain the timing as well as the temperatures of deformation and to compare these conditions to those known for shear zones of the central part of the batholith.

Orientations and senses of offset of SNB shear zones record a varying strain field during high-flux arc magmatism and subsequent cooling, displaying two distinct kinematic stages: arc-normal shortening followed by a dominant component of arc-parallel dextral shear. The timing of and sense of motion on these shear zones correspond to important changes in both the kinematics (e.g., Engebretson et al., 1985; Seton et al., 2012) and dynamics (Liu et al., 2010; Chapman et al., 2010) of Farallon plate subduction beneath the California convergent margin. The shear zones are commonly best preserved at the contacts between some of the oldest and youngest rocks of the batholith (Fig. 2), suggesting that large thermal gradients play an important role in localizing and/or preserving deformation within continental arcs. Solidified plutons such as the large swath of Triassic–Jurassic intrusives in the southeastern SNB (Fig. 2) commonly serve to pin one boundary of a shear zone, reflecting rheologic contrast between subsolidus and suprasolidus rocks.

The SNB comprises hundreds of plutons intruded over a >150 m.y. duration (e.g., Bateman, 1992), the vast majority of which were emplaced in the Cretaceous. Cretaceous plutons preserve deformation fabrics associated both with pluton emplacement and with postemplacement strain. Strain fields present during the highest flux phase of the SNB indicate that large volumes of magma were emplaced in a nonextensional setting (e.g., Tobisch et al., 1995). Beginning ca. 100 Ma, large tracts of the SNB had been emplaced and resided at elevated temperatures, creating conditions suitable for preservation of focused deformation.

The onset of dextral shear deformation within the SNB has been associated with increased rate and north azimuth of Farallon plate motion ca. 100 Ma (e.g., Glazner, 1991; Busby-Spera and Saleeby, 1990; McNulty et al., 2000; Nadin and Saleeby, 2008), as suggested by Engebretson et al. (1985). However, updated analysis by Seton et al. (2012) indicated a slightly different kinematic history for Farallon plate convergence that appears more applicable to the history of SNB shear zones. Most pertinent is a phase of generally rapid normal convergence between ca. 120 and 85 Ma, with a brief deceler-

ation between ca. 100 and 95 Ma, and a switch to overall lower convergence rates with significant dextral tangential shear ca. 85 Ma. The plate kinematic reconstructions of Seton et al. (2012) and Liu et al. (2010) also present an important plate dynamic factor, i.e., the impact and subduction of a major oceanic plateau beneath the southern California convergent margin initiating between ca. 100 and 95 Ma and progressing until ca. 85 Ma. Correlation of regional geologic structure and exhumation patterns for the southern California region (Saleeby, 2003; Saleeby et al., 2007; Chapman et al., 2010, 2012) suggests that both the dynamics of the initial impact of the oceanic plateau and its buoyancy control on slab dip are intimately related to central and southern SNB shear zone development. We thus posit that changes in both subduction kinematics and dynamics are expressed in the shear zones of the batholith.

The age of rock deformation is difficult to date directly. Ductile deformation takes place at temperature ranges that greatly exceed closure temperatures of most datable minerals that may grow during the deformation episode. As a result, a deformation date is typically an age of postdeformation cooling. Reasonable time constraints have been placed for shear zones of the SNB by combining geochronology of deformed minerals with dating of crosscutting features, and by determining deformation conditions via thermobarometry and pressure-temperature trajectories. Igneous emplacement pressures, as well as deformation temperatures revealed in this study, follow a southward-increasing trend in the southern part of the SNB (Fig. 2B), which offers an opportunity to study regional deformational features over significant depth and temperature intervals.

This study presents the first comprehensive survey of ca. 100–80 Ma Sierra Nevada thermochronometry in order to examine the regional thermal state of the batholith during formation of the major shear zones. We examine cooling from crystallization (<900 °C) through brittle-ductile transition temperatures (~300 °C). In addition, we present new <sup>40</sup>Ar/<sup>39</sup>Ar thermochronometric data constraining deformation ages of the proto-Kern Canyon and Kern Canyon faults, among the longest through-going structures of the batholith, for which there are far fewer published data than for shear zones to the north. We assess through targeted thermometry the deformation temperatures along this structure, which is obliquely exposed over ~5–30 km depths in the crust and which played a pivotal role in exhuming the deepest levels of the SNB.

## REGIONAL PLUTONIC AND TECTONIC ACTIVITY

The Sierra Nevada arc contains plutonic material as old as ca. 250 Ma (Saleeby and Dunne, 2015), but was built primarily by high-flux magmatism during Cretaceous time (e.g., Bateman, 1992; Ducea, 2001). U-Pb zircon geochronology constrains the timing of pluton crystallization throughout the batholith (Fig. 2A). A general eastward younging of pluton emplacement was resolved by U-Pb geochronology by Chen and Moore (1982), who, along with Evernden and Kistler (1970), based on their extensive biotite and hornblende

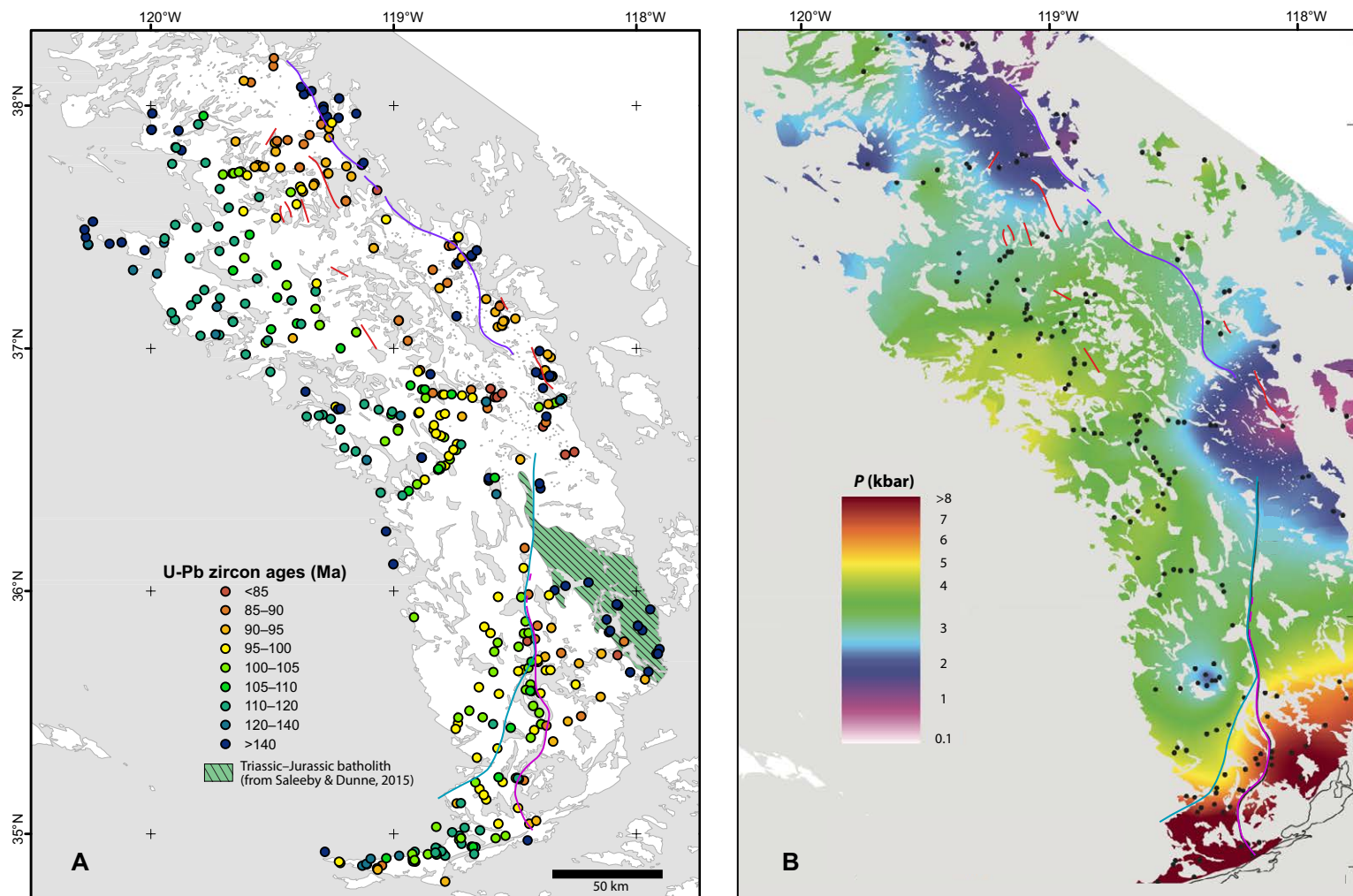


**Figure 2.** Maps of the central and southern Sierra Nevada batholith. (A) Pluton crystallization (U-Pb zircon) ages. (B) Pressures (modified from Nadin and Saleeby, 2008). Intrabatholithic shear zones are also mapped, and color coded by deformation style as in Figure 1 (see Fig. 1 for names). Note that early contractional shear zones are concentrated within the batholithic interior, while those whose deformation styles changed from contractional to dextral are localized between some of the oldest and youngest rocks of the region. On the crystallization pressure map (right), note that the proto-Kern Canyon fault follows the deepening exhumation levels of the batholith, in contrast with other transpressional shear zones that occur within and/or among shallower level plutons.

K-Ar studies, suggested that the thermal axis of the arc migrated eastward during the main Cretaceous stage of magma emplacement (ca. 120–85 Ma). However, regions of older than 120 Ma intrusives also exist in the easternmost part of the SNB (Fig. 2A), as well as in SNB rocks constituting the crystalline basement of the Great Valley (Saleeby, 2014).

Within the vast expanses of plutonic rock are prebatholithic metamorphic wall rocks that were deposited as sediments along the Paleozoic and early Mesozoic Cordilleran margin (e.g., Peck, 1980; Saleeby and Busby-Spera, 1986, 1993). These pendant rocks also commonly include unconformable remnants of Mesozoic metavolcanic and middle to late Mesozoic marine metasedimentary

rocks. In aggregate, these metamorphic framework rocks typically crop out as north-northwest–striking, steeply dipping screens and pendants (Fig. 1). A number of pendants appear to have been instrumental in localizing ductile shear for many of the central and southern SNB shear zones (Nadin and Saleeby, 2008).

Punctuating the otherwise coherent nature of the batholith are widespread deformational features that range from magmatic foliations (e.g., Bateman, 1988; Paterson et al., 2003) to the discrete ductile and brittle shear zones that we focus on here. The timing of motion on major shear zones coincides with emplacement of the largest volume of igneous material (mid- to Late Cretaceous, ca. 115–83 Ma; cf. Lackey et al., 2008), which has motivated the study of mechanisms and pathways of magma ascent and emplacement during crustal shortening (e.g., McNulty et al., 2000; Sharp et al., 2000; Paterson et al., 2011)

The 14 documented shear zones within the SNB that we concentrate on here have been interpreted to have developed as a direct consequence of subduction forcing (see Discussion and references in Table 1). These are exclusively Cretaceous structures, which commonly had low displacements (<<20 km) associated with diffuse deformation across zones >1 km wide. They are mapped in Figure 1, and their timing of motion is depicted in Figure 3 and listed along with sense of shear in Table 1. In the following we summarize published conditions of deformation, including temperatures (*T*), pressures (*P*), and senses of motion.

Sawmill Lake: 95–92 Ma; *T* < 500 °C; *P* = 2–3 kbar; contraction (Mahan et al., 2003).

Long Lake: 95–90 Ma; contraction to dextral transpression (syntectonic pluton emplacement) (Hathaway and Reed, 1994; Clemons and Bartley, 2008).

Courtright-Wishon: 94–90 Ma, *P* ~3.5 kbar, *T* = 680 to <600 °C; weak extension (Bateman, 1988; Tobisch et al., 1993, 1995; Renne et al., 1993).

Kaiser Peak: 102–91 Ma (probably closer to 95 Ma); contraction (Tobisch et al., 1995).

Quartz Mountain: 98–95 (possibly 87) Ma; *T* > 600 °C; *P* ~3 kbar; contraction (Tong, 1994; Tobisch et al., 1995).

Sing Peak: 97–98 Ma; *T* = 500–600 °C (presence of garnet; recrystallized plagioclase and orthoclase); *P* ~3–4 kbar; dextral transpression (Krueger, 2005).

Mount Hoffman: between 103 and 98 Ma; *T* > 450 °C; *P* ~2.5 kbar (Ague and Brimhall, 1988); contraction (Johnson, 2013).

Bench Canyon: 92–90 Ma with weak, domainal deformation until 78 Ma (development of pseudotachylite); *T* = 600 to <525 °C, *P* ~3.3 kbar for Mount Givens pluton (Tobisch et al., 1993); contraction to weakly extension ca. 90 Ma (Tobisch et al., 1995; McNulty et al., 2000); proposed member of the Sierra Crest shear zone system (Tikoff and de Saint Blanquat, 1997).

Virginia Canyon: 86–80 Ma; *T* from magmatic to low-*T* solid state, with brittle overprint; *P* ~2.5 kbar; dextral transpression overprinting thrust structure (Cao et al., 2015); in structural continuity with Cascade Lake.

Cascade Lake: 86–80 Ma; *T* from magmatic to low-*T* solid state (Tikoff et al., 2005); *P* ~1–3 kbar (Ague and Brimhall, 1988); dextral transpression (syntectonic with emplacement of 86 Ma Cathedral Peak Granodiorite) (Tikoff and Greene, 1994, 1997; Hutton and Miller, 1994; Fleck et al., 1996; Davis, 2010; Sharp et al., 2000; Tikoff et al., 2005); in structural continuity with Gem Lake.

Gem Lake: 91–80 Ma; *P* ~3 kbar (Ague and Brimhall, 1988); dextral transpression (in structural continuity with Cascade Lake shear zone; Segall et al.,

TABLE 1. DUCTILE SHEAR ZONES OF THE CENTRAL AND SOUTHERN SIERRA NEVADA BATHOLITH

Name	Age (Ma)	Sense of shear*	Reference
Cascade Lake	86–80	contraction --> dextral	Tikoff et al., 2005
Bench Canyon	92–90, possibly as late as 78	contraction	Tobisch et al., 1993; McNulty et al., 2000
Quartz Mountain	98–95	contraction	Tong, 1994; Tobisch et al., 1995
Gem Lake	88–80	contraction --> dextral	Segall et al., 1990; Bürgmann and Pollard, 1992; Sharp et al., 1993; Greene and Schweickert, 1995; Tikoff and Greene, 1997
Kaiser Peak	102–91	contraction	Tobisch et al., 1995
Courtright-Wishon	94–88	extension --> contraction	Bateman, 1988; Tobisch et al., 1993; 1995; Renne et al., 1993
Long Lake	94–90	contraction and/or dextral	Hathaway and Reed, 1994; Clemons and Bartley, 2008
Sawmill Lake	sometime 148–92	contraction	Mahan et al., 2003
Rosy Finch	88–83	dextral	Segall et al., 1990; Bürgmann and Pollard, 1992; Tikoff and Teysier, 1992; Sharp et al., 1993; Tikoff, 1994; Tobisch et al., 1995; Tikoff and Greene, 1997; Tikoff and St. Blanquat, 1997
Proto-Kern Canyon	95–85	contraction	Wood and Saleeby, 1998; Nadin and Saleeby, 2008
Sing Peak	97–98	dextral	Krueger, 2005
Mt Hoffman	sometime 103–98	contraction	Johnson, 2013
Virginia Canyon	86–80	contraction --> dextral	Cao et al., 2015
Kern Canyon–White Wolf	85–75, possibly younger	dextral	Busby-Spera and Saleeby, 1990; Nadin and Saleeby, 2008, 2010; Saleeby et al., 2009; Chapman et al., 2012

\*Offsets are typically <20 km, distributed across diffuse (>1 km wide) deformational zones.

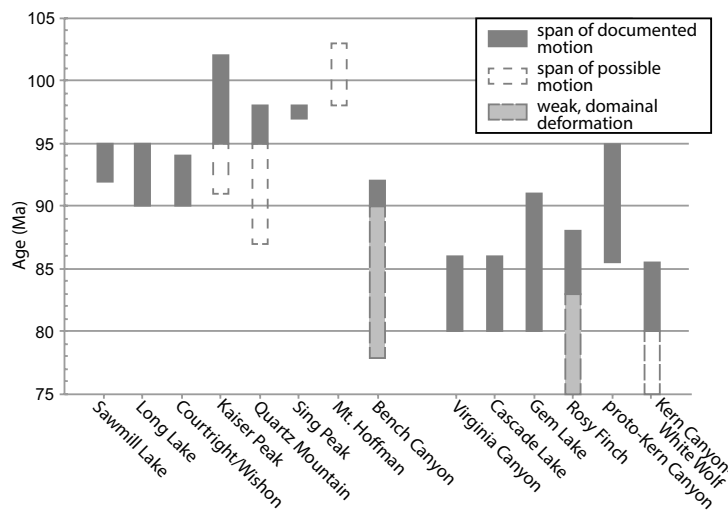


**Figure 3.** Age distribution of shear zones throughout the Sierra Nevada batholith, grouped by style of deformation. Those on the left are ca. 100–90 Ma contractional structures; those on the right are primarily 90–80 Ma contractional to dextral structures. The Kern Canyon–White Wolf fault is a dextral fault that overprints the proto–Kern Canyon fault along its northern tip.

**SUPPLEMENTAL FILE: AGES DATABASE.**

Sample Ref. #	Latitude	Longitude	U-Pb zircon age	Reference
1	37.3793	-118.6769	215	Barth et al., 2011
2	37.9493	-119.2263	218	Barth et al., 2011
3	37.4038	-118.6563	218	Barth et al., 2011
4	37.9508	-119.2843	219	Barth et al., 2011
5	37.7544	-119.1310	220	Barth et al., 2011
6	37.9966	-119.2882	221	Barth et al., 2011
7	37.9496	-119.2754	224	Barth et al., 2011
8	38.0299	-119.2245	226	Barth et al., 2011
9	37.9535	-119.2735	232	Barth et al., 2011
10	35.7412	-117.9160	91.7	Bartley et al., 2007
11	35.6359	-117.9630	93.2	Bartley et al., 2007
12	36.0351	-118.1970	147.3	Bartley et al., 2007
13	35.9237	-117.9420	165	Bartley et al., 2007
14	35.8574	-117.9930	166.1	Bartley et al., 2007
15	35.8384	-117.9740	168	Bartley et al., 2007
16	35.7605	-117.9040	176.2	Bartley et al., 2007
17	35.7415	-117.9100	182.2	Bartley et al., 2007
18	36.4500	-118.6500	98	Busby-Spera, 1983
19	36.4000	-118.5250	97	Busby-Spera, 1983
20	38.0791	-119.3636	232.9	Cao et al., 2015
21	38.0604	-119.3649	227.4	Cao et al., 2015
22	38.0686	-119.3412	220.3	Cao et al., 2015
23	38.7760	-119.8968	90.2	Cecil et al., 2012
24	38.7048	-120.0899	101.7	Cecil et al., 2012
25	38.6457	-120.1343	105.2	Cecil et al., 2012
26	38.7648	-119.8484	106.8	Cecil et al., 2012
27	38.6945	-119.9956	109.8	Cecil et al., 2012
28	38.5610	-120.2663	121.5	Cecil et al., 2012
29	38.5463	-120.3520	148.7	Cecil et al., 2012
30	38.4356	-120.5309	163.2	Cecil et al., 2012
31	38.3721	-120.5542	166.3	Cecil et al., 2012
32	34.8689	-119.0470	88	Chapman et al., 2010
33	34.8573	-119.0675	91	Chapman et al., 2010
34	34.8519	-119.0653	92	Chapman et al., 2010
35	34.8033	-118.7867	92	Chapman et al., 2010
36	35.0403	-118.4400	92	Chapman et al., 2010
37	35.0533	-118.4111	92	Chapman et al., 2010
38	34.8782	-119.2186	105	Chapman et al., 2010
39	34.8723	-119.1099	105	Chapman et al., 2010
40	34.8845	-118.9093	105	Chapman et al., 2010
41	34.8987	-119.0294	106	Chapman et al., 2010
42	34.8851	-118.9197	121	Chapman et al., 2010
43	34.8671	-119.1278	135	Chapman et al., 2010
44	34.8753	-119.1112	136	Chapman et al., 2010
45	34.8957	-119.0937	136	Chapman et al., 2010

Supplemental File. Ages database. Please visit <http://dx.doi.org/10.1130/GES01224.S1> or the full-text article on [www.gsapubs.org](http://www.gsapubs.org) to view the Supplemental File.

1990; Bürgmann and Pollard, 1992; Sharp et al., 1993; Greene and Schweickert, 1995; Tikoff and Greene, 1997).

Rosy Finch: 88–83 Ma, domainal deformation until 75 Ma;  $T = 650\text{ °C}$  to  $300\text{ °C}$  at 83 Ma;  $P \sim 3\text{--}4\text{ kbar}$ ; dextral transpression (Segall et al., 1990; Bürgmann and Pollard, 1992; Tikoff and Teyssier, 1992; Sharp et al., 1993; Tikoff, 1994; Tobisch et al., 1995; Tikoff and Greene, 1997; Tikoff and de Saint Blanquat, 1997).

Proto–Kern Canyon: 95–86 Ma;  $T = 530\text{--}415\text{ °C}$  (see discussion of results);  $P = 2\text{--}8\text{ kbar}$ ; ca. 90 Ma early contraction to dextral transpression (Wood and Saleeby, 1997; Nadin and Saleeby, 2008).

We omit the following from the study due to overlap or poor constraints. (1) Wood and Saleeby (1997) correlated the eastern Tehachapi shear zone with the southernmost segment of the proto–Kern Canyon fault. (2) The ductile to brittle dextral Farewell fault zone branches out of the Kern Canyon system at  $\sim 36.2^\circ\text{N}$  (Fig. 1; Ross, 1986; Busby-Spera and Saleeby, 1987; du Bray and Dellinger, 1988; Nadin and Saleeby, 2008). Shearing was post–98 Ma (Saleeby et al., 2007), and dextral slip is poorly constrained (Saleeby et al., 2010).

Kern Canyon–White Wolf: 86–80 Ma, possible continued motion until 75 Ma; dextral ductile shear to dextral brittle shear (Busby-Spera and Saleeby, 1990; Nadin and Saleeby, 2008, 2010; Saleeby et al., 2009; Chapman et al., 2012).

Tobisch et al. (1995) suggested that strain fields in the central SNB changed from a neutral to weakly extensional state ca. 105 Ma, to contractional ca. 100 Ma, followed by post–90 Ma dextral shearing. This study further suggested

that transition from compressive to transpressive deformation must have coincided with a change in relative plate motion between the North American and the subducting Farallon (or Kula) plates (Tobisch et al., 1995), first suggested by Engebretson et al. (1985). As summarized by the chronology of intrabatholithic shear zone activity given here (see also Table 1), those that were active prior to 90 Ma record contraction (with the exception of Courtright-Wishon and Sing Peak). Those younger than 90 Ma record dextral transpression. This deformation coincides with the apparent volumetric maxima of plutonic activity, which may have erased much of the pre–90 Ma record of regional deformation. All post–80 Ma deformation likely took place in the brittle regime.

**METHODS**

**Age Data Mapping**

A primary objective of this study is to constrain the pressure-temperature-time ( $P\text{-}T\text{-}t$ ) paths of SNB rocks during the transition from regional contraction to transpression, as recorded in the ductile shear zones that we outlined here. We examine the  $T\text{-}t$  path from (1) onset of crystallization ( $<900\text{ °C}$ , when zircon retains U and Pb; cf. Cherniak and Watson, 2001, though this is likely lower for crystallization of Sierran plutons), through (2) intermediate cooling ( $525 \pm 40\text{ °C}$ ; McDougall and Harrison, 1999), and (3) temperatures close to those of the brittle-ductile transition ( $>280\text{ °C}$ , cf. Stöckhert et al., 1999) as biotite grains close to loss of Ar ( $325 \pm 30\text{ °C}$ ; McDougall and Harrison, 1999). Other thermochronometric data for SNB rocks have been published (e.g., K-Ar muscovite), but small data sets cannot produce the batholith-wide coverage that we need to construct regional maps of thermal conditions (Figs. 2 and 4). The most comprehensive thermochronometric coverage comes from U-Pb zircon and K-Ar and  $^{40}\text{Ar}/^{39}\text{Ar}$  hornblende and biotite age data. We use the term Ar age for age-temperature data from the K-Ar and  $^{40}\text{Ar}/^{39}\text{Ar}$  data sets, which we combined because closure to Ar loss occurs within the same temperature range for both chronometers (J. Benowitz, 2014, written commun.). For consistency among data sets, we use  $^{40}\text{Ar}/^{39}\text{Ar}$  integrated ages or total gas ages (which are also sometimes reported as ages from weighted average of all heating steps).

Thus far, 487 U-Pb zircon, 250 hornblende K-Ar and  $^{40}\text{Ar}/^{39}\text{Ar}$ , and 429 biotite K-Ar and  $^{40}\text{Ar}/^{39}\text{Ar}$  ages have been published from central and southern SNB rocks (see the Supplemental File<sup>1</sup> for all compiled data). We plotted all age data sets with ArcGIS version 10.2, and cropped the figures to the region containing the major mapped shear zones. We mapped individual U-Pb zircon ages coded by color (Fig. 1), and contoured the Ar ages (Fig. 4). In Figure 2 (excluding Independence dike swarm samples), 429 U-Pb zircon ages are plotted individually because the smoothing imparted by contouring cannot fit the data: individual plutons are single age fields with sharp boundaries. Hornblende and biotite Ar ages, in contrast, can be contoured because these ages represent reheating and/or cooling that ignores sharp pluton boundaries within the batholith. The Ar age maps were created by contouring the data with a kriging regime in

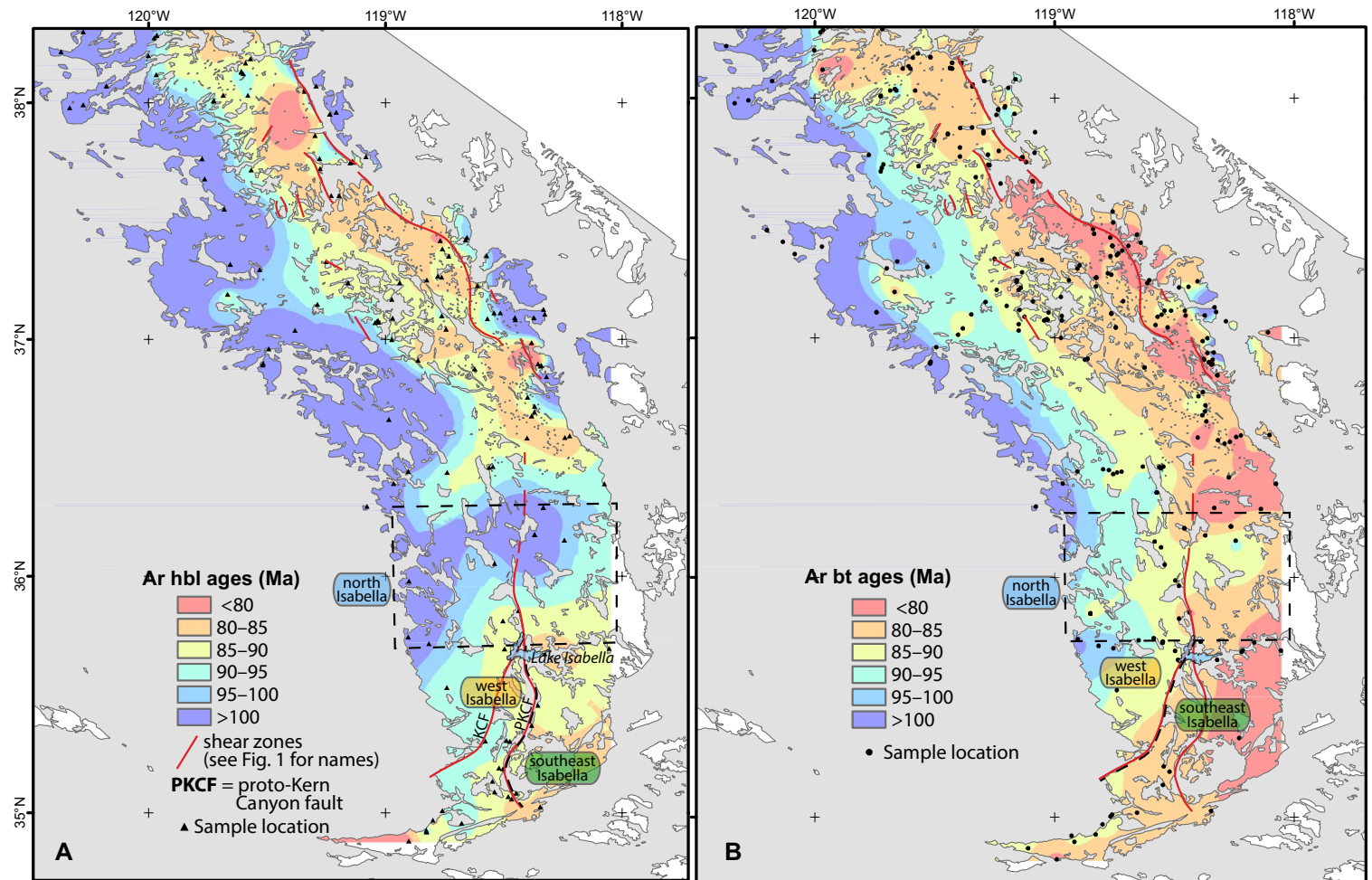


Figure 4. Color contour maps of Ar ages (including K-Ar and  $^{40}\text{Ar}/^{39}\text{Ar}$ ; see Supplemental File for data sources) with mapped shear zones. (A) For hornblende (hbl). (B) For biotite (bt). Contours were constructed with a kriging interpolator in ArcGIS v. 10.1 (described in the text). We have designated domains of the central and southern Sierra Nevada (north, west, and southeast Isabella) based on their different cooling histories (graphed in Fig. 6). These domains are named relative to Lake Isabella. The north Isabella domain covers an east-west-oriented cold, old corridor between the warm, young regions north and south of it. The southeast Isabella domain on the Ar hornblende map (A) is east of the proto-Kern Canyon fault, which in this time-temperature frame guided exhumation of the southeasternmost Sierra Nevada batholith. On the Ar biotite map (B), the southeast Isabella domain is bordered to the west by the Kern Canyon fault, which in this time-temperature frame drove extension in the southeast. The west Isabella domain includes the area west of the proto-Kern Canyon fault in A, and west of the Kern Canyon fault in B.

the ArcGIS Spatial Analyst. The parameters that best matched computed age fields (contours) with the individual ages were produced by an output cell size of 0.006, and a fixed search radius of 0.5 km with minimum 2 data points per search field.

We note here that muscovite K-Ar and/or  $^{40}\text{Ar}/^{39}\text{Ar}$  ages would help us further constrain the early thermal history of the batholith, and such ages from

K-feldspar would yield cooling rates into the brittle regime; however, we found only a few of these published dates, which is not sufficient for interpreting the thermal field of all the deformation zones within the central and southern Sierra Nevada. Few targeted zircon fission-track and (U-Th)/He age studies have been published that track local pathways into the brittle regime (e.g., Dumitru, 1990; Mahéo et al., 2009).

## Field Work and Sampling, Southern SNB Fault Zones

The proto-Kern Canyon fault is exposed along a southward-deepening transect from ~5 km paleodepths in the north to ~30 km in the south (Fig. 2B; Nadin and Saleeby, 2008, fig. 5 therein). We sampled for  $^{40}\text{Ar}/^{39}\text{Ar}$  thermochronology as well as for Ti-in-quartz and two-feldspar thermometry along this transect (Fig. 5; Table 2). We also applied Al-in-hornblende thermobarometry and plagioclase-hornblende thermometry on two samples in order to establish their crystallization pressures and temperatures.

Two samples for  $^{40}\text{Ar}/^{39}\text{Ar}$  thermochronology, LI-00B and LI-00K, were selected from the Domelands intrusive suite, which is variably deformed along the proto-Kern Canyon and Kern Canyon faults, respectively, in the vicinity of Lake Isabella (see Fig. 5 for sample locations). Sample LI-00B comes from the ca. 95 Ma granite of Cannell Creek member (Saleeby et al., 2008), which is highly deformed, with both subvertical and subhorizontal lineations in this location near the center of the proto-Kern Canyon fault. We determined hornblende, biotite, and K-feldspar  $^{40}\text{Ar}/^{39}\text{Ar}$  dates for this sample. Sample LI-00K is from the ca. 89 Ma granite of Castle Rock (Saleeby et al., 2008) that contains spaced mylonitic bands and subhorizontal lineations. We determined muscovite and K-feldspar  $^{40}\text{Ar}/^{39}\text{Ar}$  ages for sample LI-00K.

We collected 13 samples for thermometry along the proto-Kern Canyon fault from near the northern terminus to the southernmost exposures (see Fig. 5 for locations and deformation temperatures; see Table 2 for thermometric results). One sample (03H) was collected from well outside of the shear zone to determine crystallization temperature of this part of the nondeformed batholith. Of the samples, 12 were analyzed for Ti-in-quartz (TitaniQ) thermometry. Two samples (02A2 and 03H) were also analyzed for Al-in-hornblende barometry and plagioclase-hornblende thermometry (Holland and Blundy, 1994) in order to constrain the crystallization temperatures and pressures for these samples (Table 2). We did not do this for the remaining samples because in those sample locations, the batholith has been densely sampled for Al-in-hornblende emplacement pressure estimates (see Nadin and Saleeby, 2008, fig. 5 therein). Two samples (03B2 and 02A2) contained Or and plagioclase in contact with each other (Fig. 6), so we applied the two-feldspar thermometer (Benisek et al., 2004; Putirka, 2008) to test if results were consistent with the other thermometers. In sample 03B2, ductilely deformed orthoclase surrounds plagioclase (Fig. 6B), providing the opportunity to constrain feldspar deformation temperature in this location of the shear zone.

### $^{40}\text{Ar}/^{39}\text{Ar}$ Analyses

Samples for  $^{40}\text{Ar}/^{39}\text{Ar}$  analyses were crushed, sieved to 125–180  $\mu\text{m}$ , and separated using standard heavy liquid and magnetic separation methods. The  $^{40}\text{Ar}/^{39}\text{Ar}$  analyses were conducted at University of California–Santa Barbara. J-values were calculated using Taylor Creek Rhyolite sanidine with an assumed age of 27.92 Ma (Duffield and Dalrymple, 1990). Samples were step-heated in a

double vacuum resistance furnace. For K-feldspar analyses, replicate temperature steps were conducted at low to moderate steps to remove the effects of excess  $^{40}\text{Ar}$ . We assume closure temperatures of  $525 \pm 40$  °C for hornblende,  $325 \pm 30$  °C for biotite, and  $350 \pm 50$  °C for muscovite during moderate to fast cooling (see McDougall and Harrison, 1999, and references therein). K-feldspars have a complex age spectrum, which can be modeled using the multiple diffusion domain (MDD) approach to provide information on the continuous cooling history from ~300 to 150 °C (Richter et al., 1991; Harrison et al., 2005). K-feldspar diffusion data were modeled following the MDD theory and numerical approach of Lovera (1992). We assumed monotonic cooling for these models, supported by the regionally observed time intervals between zircon, hornblende, and biotite ages, and the whole-batholith-scale conductive cooling model of Barton and Hanson (1989).

### Thermometry

To constrain the temperatures of ductile deformation of the proto-Kern Canyon fault, we performed plagioclase-amphibole, two-feldspar, and/or TitaniQ thermometry for a suite of 13 samples collected along the shear zone (Fig. 5; Table 2); the type of analysis done was dictated by the mineral assemblage and applicability of the thermometer. Only samples 03H (undeformed) and 02A2 (mildly deformed) have the relevant seven-phase assemblage for Al-in-hornblende barometry. For these samples we also determined plagioclase-hornblende temperatures to correct the barometer (Anderson and Smith, 1995). Plagioclase and orthoclase feldspar from samples 02A2 and 03B2 (Fig. 5) were probed in order to apply two-feldspar thermometry, notably for sample 03B2, which contains ductilely deformed orthoclase surrounding plagioclase (Fig. 6B). All 12 sample TitaniQ temperatures were pressure corrected (Thomas et al., 2010) using the new determinations (sample 02A2) or ambient crystallization pressures determined previously (Nadin and Saleeby, 2008).

Amphibole and feldspar were measured with the Cameca SX-100 at the Brown University Geological Sciences Electron Microprobe Research Facility. For feldspar, the run conditions were beam current of 15 nA and spot size of 15  $\mu\text{m}$  (feldspar has well-known beam sensitivity), with 10 s count times. For hornblende, the beam current was 15 nA, with beam diameter at 2  $\mu\text{m}$ , and 10 s count times. Instrumental error is far outweighed by the standard deviations of pressure calculations (Supplemental File). For sample 02A2, emplacement pressure was averaged from analyses of three hornblende grains and for sample 03H two hornblende grains were analyzed. For each hornblende, at least five points were analyzed around each rim, where textural relations indicate equilibrium with quartz. We used two formulations for estimating pressure: (1) the Schmidt (1992) calculation, which determines pressure from total Al content, for consistency with preexisting data sets (e.g., Nadin and Saleeby, 2008; Chapman et al., 2012) and because of the relatively low errors associated with this calculation ( $\pm 0.6$  kbar); and (2) the Anderson and Smith (1995) calculation, which adapts the calculation for the influence of temperature on

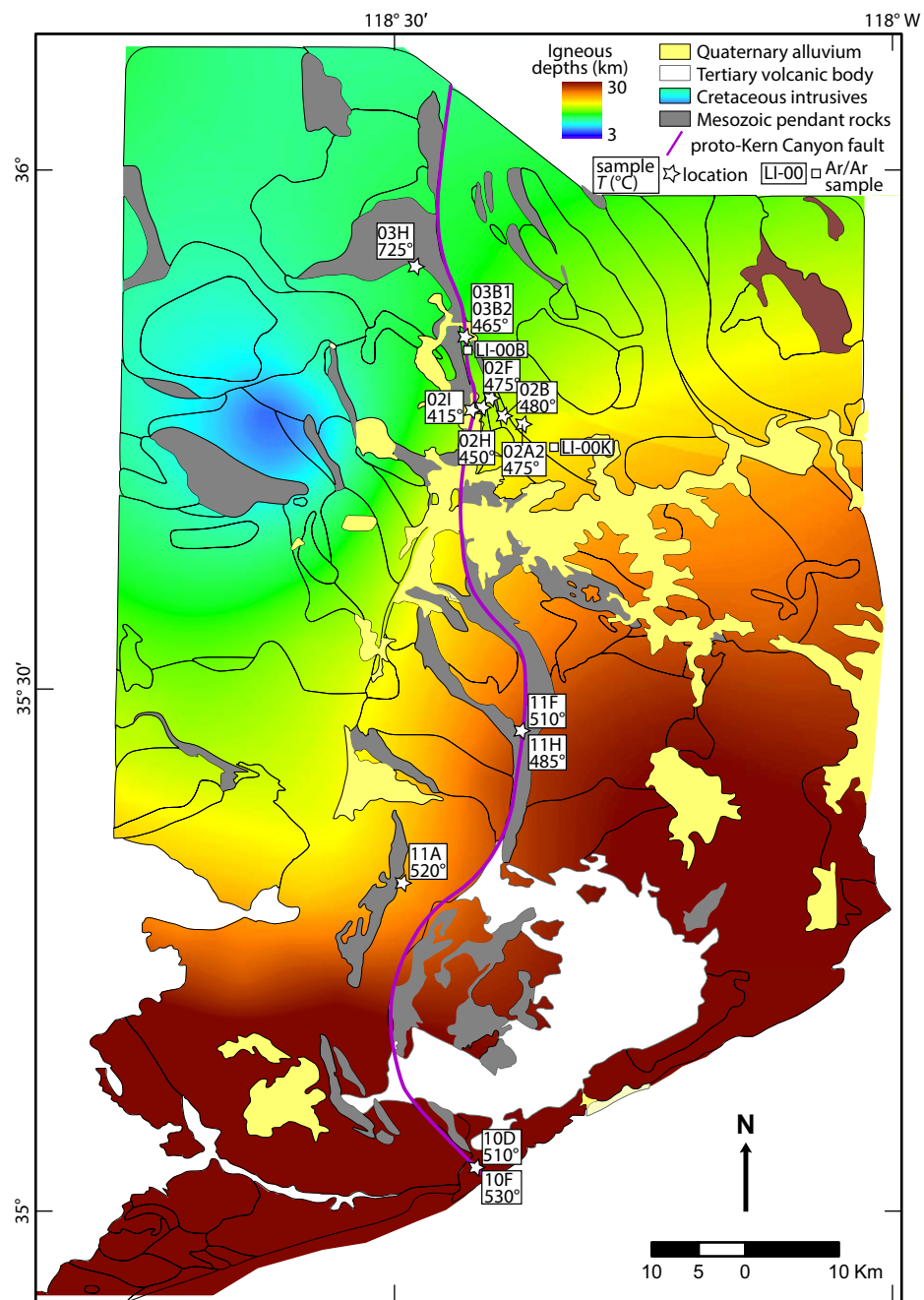


Figure 5. Sample locations for proto-Kern Canyon fault thermometry (stars) and  $^{40}\text{Ar}/^{39}\text{Ar}$  ages (small squares) mapped on an igneous crystallization depth contour surface (modified from Nadin and Saleeby, 2008). The large squares give sample numbers and temperatures from titanium-in-quartz (except for sample 03H, which shows a plagioclase-hornblende crystallization temperature from outside the shear zone). The  $^{40}\text{Ar}/^{39}\text{Ar}$  ages include hornblende, biotite, and K-spar for sample LI-00B, and muscovite and K-spar for sample LI-00K (see Fig. 7 for ages and age spectra). U-Pb zircon ages for hosting plutons are listed in Table 2, as are results from all thermometric and barometric analyses.

TABLE 2. SUMMARY OF SAMPLES ANALYZED IN THIS STUDY, INCLUDING THEIR AGES AND DEFORMATION CONDITIONS

Sample	U-Pb zircon age* (Ma)	TitaniQ† (°C)	Plagioclase-hornblende (°C)	Two-feldspar‡ (°C)	Pressure# (kbar)	Pressure** (kbar)	Depth†† (km)	Rock type
03H	102		725 ± 34		3.9 ± 0.3	3.2 ± 0.6	~11	granodiorite, undeformed
03B2	86	467 ± 30		546 ± 37			~12	granite
02A2	89	476 ± 18	725 ± 13	602 ± 58	3.9 ± 0.5	3.3 ± 0.4	~11	granodiorite
02B	94	479 ± 28					11	alaskite
02H	95	486 ± 7					~11	granite
02H2	>95	434 ± 36					~11	quartz vein
02J <sup>§§</sup>	300–200	414 ± 4					?	quartzite
02F	104	475 ± 14					12	granite
11F	103	509 ± 31					16	granite
11H	103	483 ± 41					16	granite
11A	100	523 ± 12					17	tonalite
10D	92	510 ± 20					20	granodiorite
10F	92	533 ± 29					20	granodiorite

\*Crystallization age, from Saleeby et al. (2008).

†Titanite in quartz; corrected for pressure determined via Al-in-hornblende barometry.

‡Solvcalc software (see Wen and Nekvasil, 1994) solutions: temperature,  $T_{\text{albite}} = 329 \pm 2$ ;  $T_{\text{orthoclase}} = 488 \pm 13$ ;  $T_{\text{anorthite}} = 508 \pm 31$ .

#Pressures derived from the Schmidt (1992) formula.

\*\*Pressures derived from the Anderson and Smith (1995) formula.

††Samples 03H and 02A are from this study; the remainder are from Nadin and Saleeby (2008).

§§Metamorphic pendant rock.

the pressure determination. The Anderson and Smith (1995) calculation routinely yields lower pressure estimates, which are likely more accurate because they are derived for near-solidus conditions that include H<sub>2</sub>O saturation.

Two-feldspar thermometry was undertaken for two samples, 02A2 and 03B2, which have orthoclase and plagioclase grains in contact (Fig. 5). For both samples, 2 orthoclase-plagioclase pairs were analyzed per sample, with a min-

imum of 10 spots per grain to ensure low compositional variability. We applied the Putirka (2008) formulation corrected to 3 kbar pressure to both samples. For sample 03B2 we also used Solvcalc software (Wen and Nekvasil, 1994), with crystallization pressures of 3 kbar, no change to measured compositions, and mixing models of Fuhrman and Lindsley (1988), Elkins and Grove (1990), and Benisek et al. (2004).

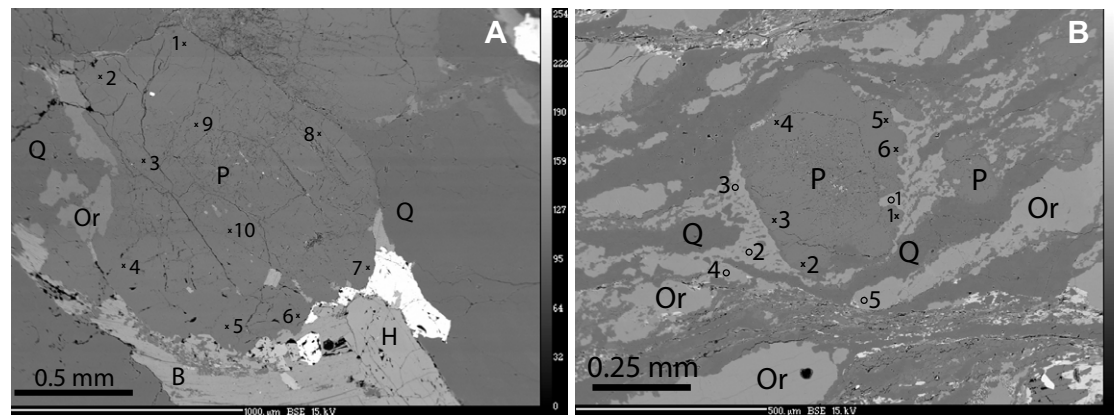


Figure 6. Backscattered electron images of mylonite samples 02A2 and 03B2 from the proto-Kern Canyon fault, showing probed spots for two-feldspar thermometry (results given in Table 2). (A) Sample 02A2. (B) Sample 03B2 shows orthoclase ductile deformed around plagioclase, suggesting that the two-feldspar temperature is that for early mylonitization. B—biotite, P—plagioclase, Q—quartz, Or—orthoclase, H—hornblende.

Concentrations of Ti in quartz were measured first with the Cameca IMS 3f ion microprobe (secondary ion mass spectrometer) at Woods Hole Oceanographic Institution (Massachusetts; WHOI) on four mylonites of the proto-Kern Canyon fault (see Table 2). We followed the procedure outlined by Wark and Watson (2006) for measuring samples with Ti concentrations below the detection limits of the more commonly used electron probe microanalysis (EPMA). These are a primary oxygen (O<sup>-</sup>) beam, current of 5–10 nA, and spot size of ~10 μm, which is less than the size of recrystallized quartz grains from the shear zone. We measured <sup>40</sup>Ca to remove peak interference from <sup>48</sup>Ca and calculate a corrected intensity of <sup>48</sup>Ti. We normalized counts on the <sup>48</sup>Ti peak to counts on reference peak <sup>30</sup>Si. Ti concentration was ultimately calculated using the corrected <sup>48</sup>Ti/<sup>30</sup>Si and the relationship between Ti (ppm) versus <sup>48</sup>Ti/<sup>30</sup>Si established for standard quartz (Wark and Watson, 2006). The Ti content of this standard (140 ppm) as measured at WHOI matched that determined by EPMA at Rensselaer Polytechnic Institute (Troy, New York).

We analyzed 9 of the 12 TitaniQ samples (Table 2) on a Cameca Sx-50 electron microprobe at the University of Alaska Fairbanks Advanced Instrumentation Lab (AIL). Reliable electron microprobe analyses require concentrations >~10 ppm (Behr et al., 2011); this requirement was met by all samples analyzed at AIL. The AIL microprobe's capability was tested by analyzing low-concentration synthetic quartz, a quartz standard used in the WHOI ion probe, and sample 03B2 (Table 2), which had been analyzed by the WHOI probe. Once we reached consistent results, we analyzed the remaining 8 samples under the following run conditions: beam current of 400 nA and spot size of 1–3 μm, acquiring elements using 3 simultaneously collecting PET (positron emission tomography) crystals for Ti Kα, and 600 s count times for peak and background for all spectrometers. Measurements were blank corrected. The 99% detection limit was 3 ppm. TitaniQ temperature estimates were calculated with the Thomas et al. (2010) expression:

$$RT \ln X_{\text{TiO}_2}(\text{quartz}) = -60952 + 1520 \cdot T(K) - 1741 \cdot P(\text{kbar}) + RT \ln a_{\text{TiO}_2} \quad (1)$$

which accounts for the pressure dependence of [Ti] in quartz, where  $R$  is the gas constant 8.3145 J/K,  $T$  is temperature in Kelvin,  $X_{\text{TiO}_2}$  (quartz) is the mole fraction of TiO<sub>2</sub> in quartz, and  $a_{\text{TiO}_2}$  is the activity of TiO<sub>2</sub>. Pressure corrections come from previously published values (Nadin and Saleeby, 2008), with the exception of sample 03H (Table 2). This sample comes from outside the proto-Kern Canyon fault, but belongs to a pluton whose margin is deformed within the shear zone. It is likely a slight overestimate of pressure because it is for crystallization conditions, and here we seek temperature of recrystallization that would occur at depth ≤ crystallization depth. A decrease in pressure of 0.5 kbar results in an ~10 °C decrease in temperature; however, it is likely that deformation began at or near crystallization conditions (see Discussion). We use an activity of Ti of 0.8 because the samples are deformed granitoids containing titanite (cf. Kohn and Northrup, 2009). Decreasing the activity to 0.6 raises the temperature by ~8 °C at the same pressure.

## RESULTS

### U-Pb Zircon Age Maps

Crystallization ages through the SNB generally decrease eastward, with a few notable exceptions (Fig. 2A). The easternmost margin of the batholith is dominated by intrusive rocks that are older than 140 Ma (some as old as ca. 248 Ma) that correspond to the earliest stages of magmatism (Chen and Moore, 1982; Chen and Tilton, 1991; Mahan et al., 2003; Bartley et al., 2007; Barth et al., 2011; Davis et al., 2012; Saleeby and Dunne, 2015). Shear zones of the east-central SNB form an apparent boundary between outcrops that contain batholithic rocks older than 140 Ma, and younger than 95 Ma intrusives. One such detailed example is from the northern terminus of the proto-Kern Canyon fault, where it intersects with an ~100-km-long belt of Jurassic and Triassic plutons (Fig. 2A; Chen and Moore, 1982; Saleeby and Dunne, 2015).

### Ar Hornblende Age Maps

As noted in the Methods discussion, we combine published K-Ar and <sup>40</sup>Ar/<sup>39</sup>Ar hornblende ages of Mesozoic intrusive rocks to produce an Ar age contour map (Fig. 4A). The SNB has a hornblende Ar age zonation similar to that of U-Pb zircon, with most ages decreasing progressively eastward with the exception of samples just east of the easternmost shear zones (Fig. 4A; see also Fig. 1 for shear zone names). The easternmost edge of the central Sierra Nevada has Ar hornblende ages older than 100 Ma. Intrusives with Ar hornblende ages younger than 90 Ma are aligned in a generally north-south-trending band in the eastern part of the batholith, with the exception of lat ~36°N, where there is an east-west swath of older than 95 Ma ages. As shown on the U-Pb zircon map (Fig. 2A), the long, through-going shear zones of the eastern Sierra Nevada appear to be localized between outcrops that have the oldest and youngest ages; in the case of Ar hornblende these are older than 100 Ma and younger than 90 Ma.

### Ar Biotite Age Maps

We combine published K-Ar and <sup>40</sup>Ar/<sup>39</sup>Ar ages for the Ar biotite age contour map (Fig. 4B). The pattern of biotite Ar ages is eastward younging, but the region of anomalously older ages shrinks to a patch just east and northeast of the Sawmill Lake shear zone. This location coincides with an area containing intrusions with older than 140 Ma U-Pb zircon ages (Fig. 2A) as well as older than 100 Ma Ar hornblende ages (Fig. 4A). Throughout the rest of the eastern edge of the batholith, Ar biotite ages are mainly younger than 80 Ma. Similar to the Ar hornblende map, there is an east-west swath of older ages near lat 36°N. The long, through-going shear zones are now located primarily within the youngest Ar biotite domains of the batholith.

## Deformation Ages and Temperatures of the Kern Canyon System

All samples for thermochronometry and thermobarometry are shown in Figure 5 and summarized in Table 2. We present here the first  $^{40}\text{Ar}/^{39}\text{Ar}$  dates and thermometry of sheared rocks along the proto-Kern Canyon fault.

### $^{40}\text{Ar}/^{39}\text{Ar}$ Thermochronometry

Sample LI-00B comes from a location (Fig. 5) where the ca. 95 Ma granite of Cannell Creek interfingers with the ca. 86 Ma Goldledge granite member (Busby-Spera and Saleeby, 1990; Saleeby et al., 2008); both are highly deformed along the center of the shear zone (Nadin and Saleeby, 2008). Because they are both intensely mylonitized where they interfinger, the two members are difficult to distinguish in the field, but in thin section the Goldledge member notably lacks hornblende. The presence of hornblende in sample LI-00B, combined with its age, suggests that the sample is from the 95 Ma granite of Cannell Creek. This sample yields a somewhat complex  $^{40}\text{Ar}/^{39}\text{Ar}$  age spectrum with climbing ages during the first 10% of gas release followed by a modest U-shaped segment for the remainder of the gas release. Although not a true plateau, the central portion of the U yields contiguous ages that compose >45% of the gas and yield a weighted mean plateau age of  $89.1 \pm 0.1$  Ma or 14 point isochron age of  $88.8 \pm 0.2$  Ma (Fig. 7; mean square of weighted deviates,

MSWD = 1.11). The biotite from this sample yields a similarly shaped age spectrum (Fig. 7) that flattens over the last 50% of gas release. The 6 point isochron age of  $79.1 \pm 1.0$  Ma (MSWD = 1.83 and  $^{40}\text{Ar}/^{36}\text{Ar} = 397.7 \pm 94.2$ ) is similar in age to the flat portion of the age spectrum. The K-feldspar age gradient climbs from ca. 69 Ma at low-temperature steps to ca. 79 Ma at high-temperature steps (Fig. 7). The K-feldspar diffusion data were best fit by 7 discrete domain sizes and an activation energy,  $E = 47.00$  kcal/mol. Combined age results and best-fit MDD models suggest that this sample cooled linearly, from 250 to 175 °C, at a moderate rate ( $\sim 15$  °C/m.y.) from 89 to 71 Ma. Moderate cooling was followed by very slow cooling ( $\sim 1$  °C/m.y.) to 150 °C until at least 69 Ma. We note here that because of interfingering with the 86 Ma Goldledge granite, there was probably reheating at 86 Ma and the cooling path is probably not linear.

The second sample came from  $\sim 5$  km north of Lake Isabella (sample LI-00K; see Fig. 5 for location) from the ca. 89 Ma granite of Castle Rock granite member of the Domelands intrusive suite (Saleeby et al., 2008). In this location within the Kern Canyon fault, deformation is distributed as pervasive modest grain-size reduction and concentrated mylonitic shear bands with horizontal lineations attesting to dextral shear. Sample LI-00K is therefore moderately deformed, with quartz, feldspar, and micas flattened into parallelism. Muscovite from this pluton yields a nearly flat  $^{40}\text{Ar}/^{39}\text{Ar}$  age spectrum with a plateau age of  $82.3 \pm 0.1$  Ma (Fig. 7B). The K-feldspar age spectrum climbs from 67 Ma at low-temperature steps to ca. 78 Ma at high-temperature steps. K-feldspar diffusion data from this sample were best modeled with 8 discrete domain

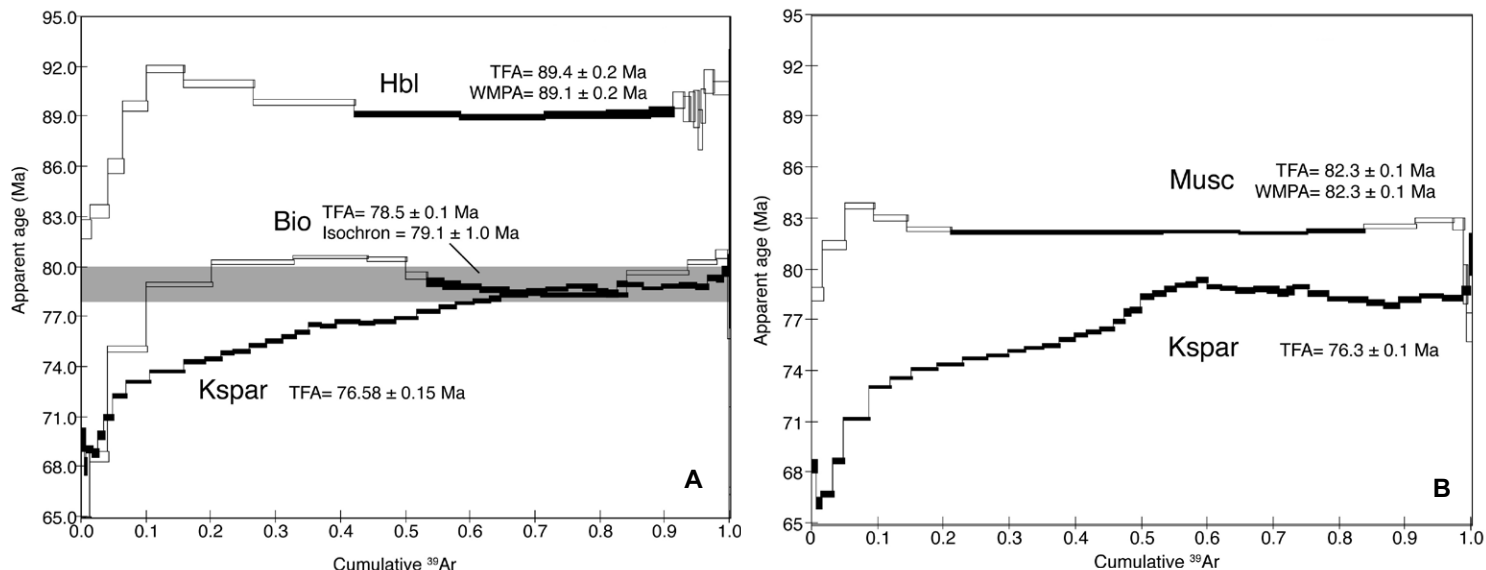


Figure 7. (A)  $^{40}\text{Ar}/^{39}\text{Ar}$  age spectra for samples (A) LI-00B hornblende (Hbl), biotite (Bio), and K-feldspar (Kspar) of the ca. 95 Ma granite of Cannell Creek, and (B) LI-00K muscovite (Musc) and Kspar of the ca. 89 Ma granite of Castle Rock. TFA—total fusion age; WMPA—weighted mean plateau age.

sizes and  $E = 47.53$  kcal/mol (Fig. 7B). Combined thermochronologic data from this pluton suggest moderate (14–17 °C/m.y.) cooling from ~350–165 °C from 82 to 70 Ma, followed by very slow cooling (~1 °C/m.y.) to <150 °C after 70 Ma.

### Thermometry

Figure 5 shows sample locations and TitaniQ temperatures for all samples selected for thermometry, in the context of the ambient igneous crystallization depths. Other thermometric results given in the text and Table 2, but not shown in Figure 5, were derived from plagioclase-hornblende and two-feldspar measurements.

Both the Schmidt (1992) and the Anderson and Smith (1995) formulations of the Al-in-hornblende thermometer indicate that samples 02A2 and 03H (see Fig. 5 for locations) crystallized at ~3–4 kbar, or >10 km depth (Table 2). Both calibrations have an associated  $\pm 0.6$  kbar external error, which is greater than the  $\pm 0.3$ – $0.6$  kbar standard deviations for both samples. Sample 02A2 is mildly deformed granite of Castle Rock with weak foliation and ribboned quartz, dated at 88 Ma (Saleeby et al., 2008). It yielded crystallization pressures of  $3.9 \pm 0.5$  kbar (Schmidt, 1992) or  $3.3 \pm 0.4$  kbar (Anderson and Smith, 1995) and plagioclase-hornblende (crystallization) temperatures of ~725 °C via the Blundy and Holland (1990) thermometer. Sample 03H is from the nondeformed 104 Ma granite of Kern River (Saleeby et al., 2008) and yields crystallization pressures of  $3.9 \pm 0.3$  kbar (Schmidt, 1992) or  $3.2 \pm 0.6$  kbar (Anderson and Smith, 1995) and temperatures ~725 °C.

Sample 02A2 and 03B2 two-feldspar thermometry (Fig. 6) yielded temperatures of  $604 \pm 44$  °C and  $508 \pm 89$  °C, respectively, for K-spar crystallization using the global regression model of Putirka (2008). Sample 03B2 was analyzed more extensively because of its possible value in recording feldspar recrystallization temperature (Fig. 6B). The Solvcalc solution yielded  $T_{\text{orthoclase}} \sim 477$ – $502$  °C from the Fuhrman and Lindsley (1988), Elkins and Grove (1990), and Benisek et al. (2004) formulations.

Quartz recrystallization temperatures along the proto-Kern Canyon fault, for the 12 samples collected along the shear zone (Fig. 5; Table 2), range from 415 to 530 °C. These deformation temperatures increase from north to south along the same trend as increasing igneous crystallization depths (Fig. 2B). Sample 02H2 is from a quartz vein that is transposed into the foliation plane of its host granodiorite, and was completely dynamically recrystallized (sample 02H). In this case, the two have nearly overlapping TitaniQ temperatures of  $486 \pm 7$  °C for the host pluton and  $434 \pm 36$  °C for the sheared vein (Table 2). A quartzite from a metamorphic pendant (sample 02I) was also measured, and yielded a TitaniQ temperature of ~415 °C.

## DISCUSSION

The wealth of data produced for the SNB by numerous investigators has allowed for fairly detailed geological interpretations, which continue to be revised. Often the scope of a single inquiry is focused by necessity, given the size

and time span encompassed by rocks of the batholith. In this study we incorporate information from several sources as well as present new data to examine the thermal evolution of the southern half of the batholith over a >20 m.y. time span. We then evaluate the timing and deformation style of major shear zones in the context of the evolving thermal conditions.

Many studies of SNB magmatism support the idea that the batholith was assembled via magmatic flare-ups that peaked ca. 225 Ma, 161 Ma, and 98 Ma (see Cao et al., 2015, fig. 15 therein). Targeted inquiries certainly support the case for discrete magma pulses (Stern et al., 1981; Chen and Moore, 1982; Frost and Mattinson, 1993; Coleman and Glazner, 1998; Ducea, 2001; Coleman et al., 2004; Ducea and Barton, 2007; DeCelles et al., 2009; Paterson and Ducea, 2015; Ducea et al., 2015). However, a comprehensive table of U-Pb zircon ages shows that there was never a complete cessation of magmatism, or any significant lulls, from ca. 140 to 84 Ma (Supplemental File; Saleeby and Sharp, 1980; Chen and Moore, 1982; Saleeby et al., 2007; Lackey et al., 2008; Cecil et al., 2012; Chapman et al., 2012; Saleeby, 2014; deSilva et al., 2015), the time interval relevant to development of the preserved shear zones discussed herein. The U-Pb zircon age database and map (Fig. 2; Supplemental File) by no means represents the volume of material emplaced at different ages, but it serves to identify the timing of magmatism in the batholith. In the central and southern SNB, the majority of ages are in the most recent stage of activity (62% of ages are 110–80 Ma), but 22% of the samples are in the 140–110 Ma time interval that is outside the peak in Sierra Nevada plutonism. Significant tracts of 140–110 Ma Sierran intrusives nonconformably underlie upper Cretaceous forearc basin strata in the Great Valley subsurface (May and Hewitt, 1948; Saleeby, 2007, 2014). This large tract of batholithic material is distal to the shear zones that we focus on here, thus allowing us to focus on the mid- to Late Cretaceous thermal evolution of the exposed batholith, which is most pertinent to the shear zones.

An effectively uninterrupted magma supply for mid- to Late Cretaceous time provides the continuous record needed to examine the styles and locations of shearing through the batholith that we posit were controlled by stress, temperature, and horizontal temperature gradients. In addition, new sources of magma provided focused heating that may have guided such deformation.

## Thermotectonic History

### Regional SNB Thermal History

The data presented here offer the opportunity to interpret the high- to medial-range thermal history of the southern and central SNB (Fig. 4). These maps may also serve to guide further sampling that may provide better insight into the thermal and structural history of the batholith.

Because plutonic activity was uninterrupted in the central and southern SNB from ca. 140 to 85 Ma, postemplacement cooling was probably quite variable in different regions, and protracted and punctuated by reheating as

new intrusions were emplaced. The timing of cooling was primarily controlled by the ages of igneous emplacement, such that regions that cooled earlier were regions with older plutons, and regions that stayed warmer longer had younger superposed plutonism. In addition, older, cooled terrane could be reheated by subsequent voluminous plutonism. We consider reheating by individual intrusions to be negligible for our primary focus given the scale of the major batholithic zones and their regional cooling patterns (as suggested by the conductive cooling model of Barton and Hanson, 1989).

In this study we depict three main age-temperature data sets, U-Pb zircon (~900 °C), Ar hornblende (~525 °C), and Ar biotite (~325 °C), in order to explore the regional pattern of cooling in the SNB (Figs. 2 and 4) through brittle-plastic transition temperatures. The older western margin of the batholith cooled early and remained cold, while the eastern side was continuously resupplied with magma and cooled more slowly. This general picture is punctuated by two local thermal breaches just north of lat 36°N. The first is the Mount Whitney Intrusive Suite which includes the youngest (ca. 84 Ma) and shallowest ( $P \sim 1$  kbar) plutonism in the batholith. The suite is centered at the southeast termination of the Sawmill Lake shear zone (Fig. 2A) and is especially notable as the ellipse of shallowest emplacement pressures shown in Figure 2B. The second thermal anomaly is seen most clearly on the hornblende Ar age map (Fig. 4A): an east-west-oriented corridor just north of lat 36°N, which cooled earlier than 100 Ma, in contrast with the surrounding regions that cooled ca. 85–80 Ma. The corridor is well defined east of the Kern Canyon fault, where three samples come from Triassic–Jurassic plutons whose map extents are significant (Fig. 2A; Saleeby and Dunne, 2015).

The paired Mount Whitney Intrusive Suite high-temperature and 36°N cool corridor suggest that a thermal barrier segregated the southernmost shear zones (Kern Canyon–White Wolf fault system) from those to the north. The Mount Whitney Intrusive Suite was likely responsible for heating surrounding rocks above the biotite Ar closure temperature (or slowing their cooling paths), but the older, colder region persisted somewhat through this temperature, due primarily to an abundance of early Mesozoic intrusions in the area (Fig. 2; Saleeby and Dunne, 2015). An additional noteworthy feature on the biotite Ar age map is a zone of rocks that cooled more recently (ca. 80–70 Ma biotite Ar ages) in the southeasternmost part of the batholith. This swath suggests a structural connection to the Kern Canyon fault on its western border; we explore this in the following, where we attempt to place the deformational history into the context of temperature distribution. We also note that the 80–70 Ma swath on the biotite Ar age map coincides with the area of temperature closure through (U-Th)/He zircon (~190 °C) between 80 and 70 Ma, signaling rapid cooling through medial temperatures (Chapman et al., 2012). The map distribution of this swath suggests a thermal-tectonic control by the Kern Canyon system, which we explore in the following.

In order to explore the seemingly different cooling history of the southern SNB from regions northward, we split the southern part into three different thermotectonic zones. We consider the “cool corridor” (Fig. 4A) to define a northern province, coinciding with the northern terminus of the Kern Canyon

fault at lat 36.3°N. South of this (lat ~35.5°N), in the time frame during which cooling proceeded through ~525 °C, the proto–Kern Canyon fault guided exhumation of the southeasternmost part of the batholith. We thus designate a southeast Isabella geographic province eastward of the proto–Kern Canyon fault. The west Isabella province extends westward from the proto–Kern Canyon fault to the western edge of the exposed batholith. As the southern part of the batholith emerged due to local forces through ~325 °C, the Kern Canyon fault became the driver for extension in the southeast, and thus this structures defines the border between the west Isabella and southeast Isabella domains after ca. 85 Ma (Fig. 4B).

The cooling histories of these three provinces (Fig. 8) are overlapping but distinctive. The U-Pb zircon age data are shown for the context of the earliest thermal history; they span a large age range but follow the general pattern of oldest to the north and youngest to the southeast, suggesting that different tectonic processes were responsible for their cooling paths. North Isabella underwent protracted cooling throughout its history because it contains plutons that range in age from 248 to 84 Ma. Average hornblende Ar ages here are  $104 \pm 12$  Ma, and biotite Ar average ages are  $87 \pm 6$  Ma. West Isabella cooled later and more rapidly, with identical average hornblende Ar and biotite Ar ages, ca.  $91 \pm 6$  Ma. Southeast Isabella cooled even later, going from hornblende Ar temperatures at  $85 \pm 4$  Ma to biotite Ar temperatures at  $82 \pm 3$  Ma.

### ***Proto–Kern Canyon and Kern Canyon Fault Thermal Histories***

We explore the thermal history of the proto–Kern Canyon fault in detail to compare and contrast the deformational history of this major shear zone to the more spatially restricted shear zones to the north.

In the central part of the shear zone, pluton crystallization temperatures extended down to ~725 °C, as indicated by plagioclase-hornblende thermometry (Fig. 5; Table 2; samples 03H and 02A2). Deformation started under hot subsolidus conditions at temperatures at least 450–600 °C, as suggested by ductilely deformed feldspars (Passchier and Trouw, 2005) of sample 02A2 (Fig. 6A), from the mildly deformed ca. 89 Ma granite of Castle Rock (Saleeby et al., 2008). Sample LI-00K, which comes from the same granite body, moderately deformed along the Kern Canyon fault, has deformed muscovite with a  $^{40}\text{Ar}/^{39}\text{Ar}$  age of ca. 82 Ma. Muscovite  $^{40}\text{Ar}/^{39}\text{Ar}$  ages correspond to deformation temperatures near 450 °C, and this deformation temperature is confirmed by the ~475 °C TitaniQ result from ductilely deformed quartz of nearby samples 02A2 and 02B (Fig. 5). Sample LI-00B, from the 95 Ma granite of Cannell Creek, contains 89 Ma deformed hornblende as well as 80 Ma deformed biotite. This information, along with TitaniQ temperatures from mylonitized sections of the Goldledge, Cannell Creek, and Castle Rock granites and quartz veins that are transposed into alignment with S surfaces, suggest that deformation took place during cooling from >500 to 450 °C. An array of  $T-t$  data from plutons that were deformed during cooling suggest a protracted interval of shearing from at least 90 to 80 Ma, during which time proto–Kern Canyon transpres-

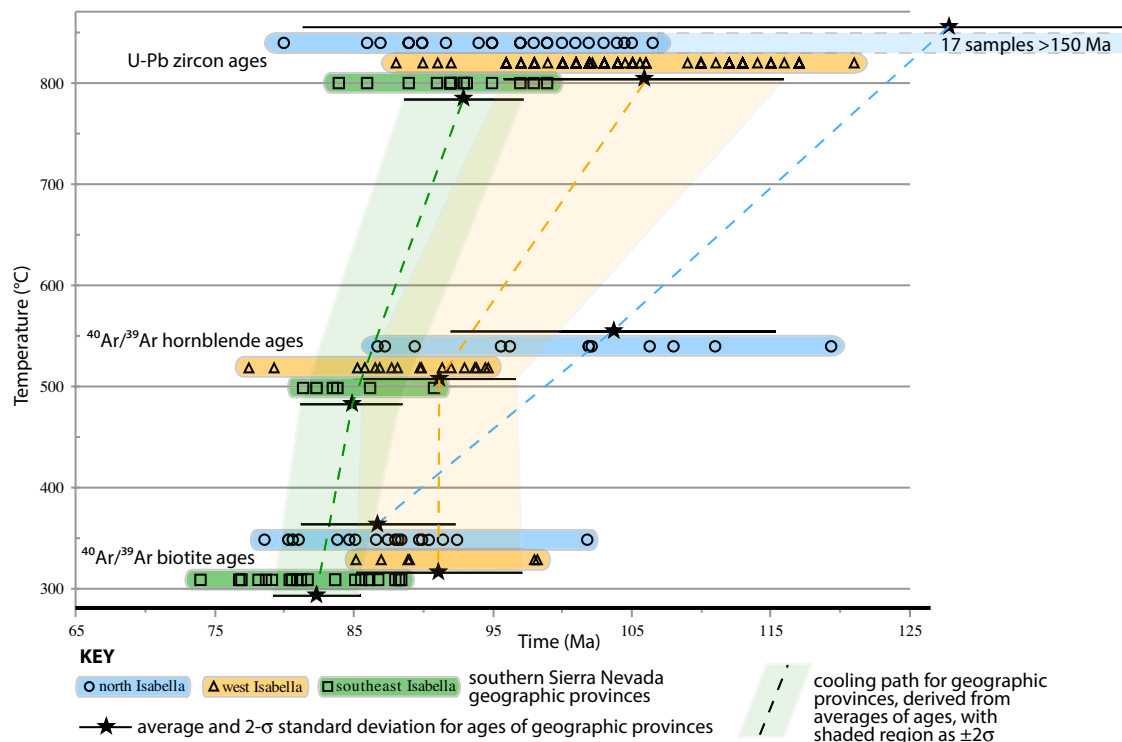


Figure 8. Cooling paths for the north (blue), west (orange), and southeast (green) domains of the central and southern Sierra Nevada batholith (delineated in Fig. 4). Each colored horizontal bar encircles the full spread of sample ages for U-Pb zircon (~900 °C), Ar hornblende (~525 °C), and Ar biotite (~325 °C) from the corresponding domain. The pathways between the temperatures are depicted by a dashed line that connects average ages (marked by a star), and a swath whose width corresponds to the 2σ calculated standard deviation. The west and southeast Isabella domains cooled rapidly from 525 to 325 °C.

sional deformation ceased and was overprinted by Kern Canyon fault dextral shearing. Shearing in the ductile regime ended as these rocks cooled through ~450 °C, as recorded by TitaniQ thermometry.

The southern part of the proto-Kern Canyon fault records higher TitaniQ deformation temperatures of 485–530 °C. We interpret these higher temperatures to indicate that deformation in the ductile regime along this segment of the fault ceased earlier, “freezing in” the deeper record of the shear zone in this area possibly as a result of rapid exhumation in the south (e.g., Chapman et al., 2010, 2012, and references therein). Figure 8 shows that the region north of Lake Isabella cooled much more slowly than the region to the south, particularly after ca. 90 Ma. Another potential factor in controlling this pattern is that ca. 85 Ma, the northern proto-Kern Canyon fault was abruptly overprinted by the northern reaches of the dextral Kern Canyon–White Wolf system (Fig. 1).

### Cooling Rates of Central SNB Shear Zones

Sheared plutons are crucial to placing temporal and thermal constraints on strain localization, as well as on the ambient cooling history of the deforming region. One well-studied example in the central region of the SNB

is the Courtright shear zone, an early compressional structure that developed between large plutons that are ca. 102 and ca. 90 Ma (Renne et al., 1993). U-Pb zircon and <sup>40</sup>Ar/<sup>39</sup>Ar (hornblende and biotite) ages of minerals, as well as plagioclase-hornblende thermometry, from the two plutons and from the intervening shear zone suggest that activity began during ca. 90 Ma pluton emplacement at a subsolidus temperature of 680 °C (Renne et al., 1993; Tobisch et al., 1993). Recrystallized biotite from the shear zone is dated as 88.7 Ma. These data suggest very rapid cooling of ~130 °C/m.y. between 500 and 300 °C (Renne et al., 1993) at the tail end of compressive deformation.

In the east-central SNB, the recently mapped Virginia Canyon shear zone deforms a ca. 86 Ma pluton, which was emplaced at ~2.5 kbar and ~700 °C (Cao et al., 2015, and references therein). It is also continuous with the Cascade Lake shear zone to the south, which was active from 86 to 80 Ma (e.g., Tikoff et al., 2005). Cao et al. (2015) suggested that the Virginia Canyon shear zone entered the brittle regime (300 °C) at 80 Ma. The <sup>40</sup>Ar/<sup>39</sup>Ar ages of hornblende and fine-grained biotite from the shear zone hosting pluton are 86 Ma and 80 Ma, respectively. Together, the age-temperature estimates suggest a cooling rate of ~35 °C/m.y. from 530 to 330 °C, which is likely more representative

of the broader region than the rapid cooling rate derived from the vicinity of the Courtright shear zone.

In the southern SNB, where the Kern Canyon–White Wolf fault merges with the proto–Kern Canyon fault in the vicinity of Lake Isabella, the integrated hornblende, biotite, and K-spar  $^{40}\text{Ar}/^{39}\text{Ar}$  thermometry (samples LI-00K and LI-00B) suggests a cooling rate similar to that of the Virginia Canyon–Cascade Lake system: a moderate rate of  $\sim 30$  °C/m.y., from  $\sim 640$  to  $360$  °C over the interval 92–82 Ma. This was followed by slower rates of  $\sim 17$  °C/m.y. until ca. 70 Ma and afterward ( $\sim 1$  °C/m.y.).

Noting the different cooling rates calculated for specific domains of intrabatholithic shear zones, and considering that these deformation zones commonly overprint intrusives that span a wide age range, it seems evident that a single cooling rate would likely not apply to a single, aerially extensive shear zone. In the vicinity of the proto–Kern Canyon fault, the Goldledge granite cooled quite rapidly, for example, from syntectonic emplacement at 86 Ma through biotite Ar closure at 80 Ma. The cooling rate for this intrusive is therefore  $\sim 70$  °C/m.y. This higher cooling rate is consistent with cation distribution modeling of feldspar from deformed sample 03B2, whose K content of plagioclase is relatively high and suggests limited Na-K diffusion associated with higher cooling rates (A. Benisek, 2014, written commun.).

The southern segment of the proto–Kern Canyon fault (south of Lake Isabella; Fig. 1) underwent more rapid cooling than the segment to the north. Thermobarometric and thermochronometric data (Nadin and Saleeby, 2008; Maheo et al., 2009; Blythe and Longinotti, 2013; Chapman et al., 2012) show that from 90 to 80 Ma, the area south of Lake Isabella cooled and decompressed from  $>650$  °C and  $\sim 6$  kbar to  $\sim 180$  °C ca. 80 Ma, and continued cooling rapidly through apatite (U-Th)/He until ca. 70 Ma. In the following discussion of drivers for cooling we discuss the kinematic framework of intrabatholithic deformation in greater detail, but here we suggest that low-angle displacement along the underlying Rand fault in the southernmost part of the batholith (e.g., Chapman et al., 2010, 2012) is directly responsible for exposing rocks deformed at higher temperatures, as well as for the higher cooling rate along the southern proto–Kern Canyon fault.

### **Tectonic History**

Exposures of the central and southern SNB are dominated by plutons that were emplaced between 110 and 85 Ma (Fig. 2), and thus it follows that mid- to Late Cretaceous intrabatholithic shear zones were preferentially preserved in this region. We recognize that Early Cretaceous synplutonic shear zones operated in the southern SNB region (Bateman et al., 1983; Tobisch et al. 1989; Clemens-Knot and Saleeby, 1999), although these are limited in aerial extent due to intrusive truncations by more voluminous mid- to Late Cretaceous plutons. We focus here on principally Late Cretaceous intrabatholithic shear zones of the central to southern SNB, for which the deformation record is fairly continuous from 100 to 80 Ma. In the central Sierra Nevada (north of

lat  $36.5^\circ\text{N}$ ), ductile shear zones like Quartz Mountain, Bench Canyon, Courtright, and Kaiser Peak, which show mainly arc-normal shortening with minor superimposed local extension, developed between 100 and 90 Ma (Table 1; McNulty, 1995; Tobisch et al., 1995; McNulty et al., 2000). These shear zones are preserved as relatively short ( $<25$  km long) structures through the axial zone of the batholith (Fig. 1). In contrast, long through-going ductile shear zones are well preserved along the eastern edge of the central SNB, where ca. 90 Ma plutons record the transition from regional contraction to dextral transcurrent shear (Cao et al., 2015; Tobisch et al., 1993, 1995; Renne et al., 1993; McNulty et al., 2000; Sharp et al., 2000). The Virginia Canyon, Cascade Lake, Gem Lake, and Rosy Finch shear zones are along strike of one another and are also along the boundary between plutons that are older than 140 Ma to the east and younger than 100 Ma to the west. Older intrusives show steeply plunging lineations consistent with transverse shortening, and younger, syntectonic granites record shallowly plunging lineations consistent with tangential shear (Tikoff and Teysier, 1992; Greene and Schweickert, 1995; Tikoff and de Saint Blanquat, 1997; Tikoff and Greene, 1997; Tikoff et al., 2005).

Structural relations along the contiguous Cascade Lake–Gem Lake shear zones indicate highly variable finite strain along strike (Tikoff and Greene, 1997). The Rosy Finch shear zone has an order of magnitude lower shear-strain values than in the Gem Lake shear zone to the north ( $\gamma = 20$  for Gem Lake versus  $\gamma \sim 2$  for Rosy Finch; Tikoff and Greene, 1997). Similarly, the proto–Kern Canyon fault has much higher strain in the south, as well as greater thrust and strike-slip displacements (Wood, 1997; Nadin and Saleeby, 2008) accompanying the higher deformation temperatures reported here.

Although the Rosy Finch shear zone has been suggested to link with the proto–Kern Canyon fault as part of the Sierra Crest shear zone system (e.g., Tikoff and de Saint Blanquat, 1997), no physical continuity between the two has been mapped. Given the evidence for decreasing shear strain and offsets of both shear zones as they converge in the vicinity of the Mount Whitney Intrusive Suite, as well as evidence for a thermal barrier, we suggest that the Virginia Canyon, Cascade Lake, Gem Lake, and Rosy Finch shear zones in the central Sierra Nevada arose under a different tectonic regime than did the proto–Kern Canyon fault to the south. This finding is further supported by (1) the 4–9 m.y. differences in ages of initiation and termination of the proto–Kern Canyon fault and faults of the Sierra Crest shear zone system (Fig. 3), and (2) an  $\sim 40^\circ$  discordance between the regional strike of the Sierra Crest system and the northern segment of the overlapping proto–Kern and Kern Canyon systems.

### **Drivers for Cooling and Deformation**

Many plate kinematic discussions cite the Engebretson et al. (1985) model that invokes a doubling of Farallon plate speed and  $10^\circ$  change in obliquity of plate convergence between 100 and 90 Ma. More recent estimates of relative

plate motion from Cao et al. (2015), who used orientations of deformed bedrock, support a transition from normal- to oblique-sense convergence between 97 and 90 Ma. Updated global plate motion models (Seton et al., 2012) provide greater time resolution, in 5 m.y. time steps of Farallon–North America convergence rates and directions (Fig. 9) of relative plate motion. Furthermore, many recent studies suggest that more local features influenced the timing and kinematics of subduction-driven deformation (e.g., oceanic plateau subduction). We pursue these kinematic and dynamic features here, as they attest to the structural complexity that is manifest in the batholith.

In the Seton et al. (2012) reconstruction (Fig. 9), the convergence rate between the Farallon and North American plates (at southern SNB latitudes) increased abruptly ca. 120 Ma, and remained high (~100 mm/yr) at nearly normal convergence until ca. 100 Ma, when convergence rates dropped abruptly for ~5 m.y. Over the 120–85 Ma interval, modest tangential components of convergence changed from sinistral through nil to dextral (Fig. 10). The ca. 95 Ma convergence rates accelerated to as high as ~150 mm/yr, and then dropped back to ~100 mm/yr ca. 85 Ma, when dextral tangential components increased significantly.

The plate kinematic reconstruction places the SNB in a continuously compressional setting from 120 to 85 Ma. At 100 Ma, when Farallon plate velocity dropped, the magmatic front moved eastward (Fig. 2A), and arc-normal shortening led to formation and preservation of the compressional Quartz Mountain, Bench Canyon, Courtright, and Kaiser Peak shear zones (Fig. 10A). This is counter to what is commonly assumed, that magmatic front migration is

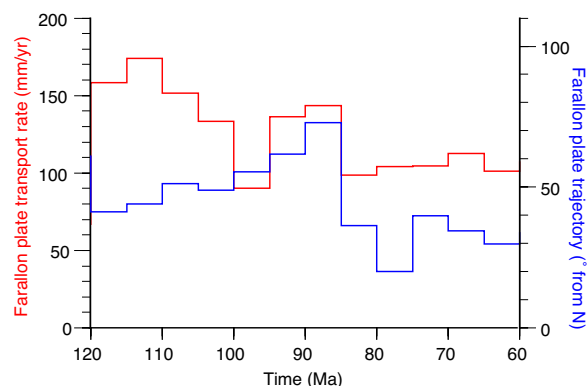


**Figure 9.** Reconstruction of Farallon–North America convergence direction (blue line) and rate (red line) from 120 to 60 Ma showing the detailed convergence history derived from Seton et al. (2012); highlights are briefly summarized in the text. The ca. 85 Ma drop in convergence rate and direction of the Farallon plate coincides with a major change in the deformational regime of the Sierra Nevada batholith, from compressional to dextral shearing. The trajectory of the Farallon plate is given in degrees from north. Note that in Figure 10 the relative convergence direction is adjusted for the N30W orientation of the Sierra Nevada batholith during this time interval.

driven by acceleration in convergence rates (Dickinson and Snyder, 1978). This seemingly extraordinary regime of arc migration and intensified contractile deformation coincident with deceleration in convergent rates coincided with the impact of the Shatsky Rise conjugate, a large oceanic plateau that was embedded within the Farallon plate and that subducted beneath the California convergent margin in the Late Cretaceous (Saleeby, 2003, fig. 4 therein; Chapman et al., 2010; Liu et al., 2008, 2010).

We posit that initial impact of the Shatsky Rise conjugate between 100 and 95 Ma (Liu et al., 2010, fig. 1 therein) initially slowed Farallon plate subduction due to increased traction from slab flattening and tectonic erosion of the SNB mantle wedge (Saleeby, 2003). Between ca. 95 and 90 Ma, the thickened basaltic crust of the Shatsky Rise conjugate reached eclogite facies conditions deeper in the subduction zone and became negatively buoyant, leading to the subsequent acceleration in plate convergence. The 100–90 Ma time interval coincides with arc-normal shortening dominating the central to southern SNB upper plate. Spatial and temporal complexities in the initial impact and ensuing subduction of the Shatsky Rise conjugate likely arose from the primary structure and bathymetry of the rise. Most pertinent is a profound bathymetric gradient that formed across the principal igneous massif and its broad shoulders (Sager, 2005). According to contemporary Shatsky Rise bathymetry and the reconstruction of the conjugate as it impinged on the California convergent margin, the steep bathymetric gradient maps onto the southern SNB. This imparted three profound regional structural imprints: (1) at the southern end of the SNB and continuing southward into the Mojave region, the entire mantle wedge of the SNB was sheared off and replaced by subduction accretion assemblages (Saleeby, 2003; Chapman et al., 2010), while further north in the SNB the mantle wedge was left intact; (2) a north-dipping lateral ramp in the Rand to Coast Range (Franciscan) subduction megathrust developed, above which the strong southward depth of exhumation gradient in the southernmost SNB developed (Fig. 2B); and (3) the proto–Kern Canyon fault developed as a whole-crust–penetrating lateral ramp that climbed northward out of the Rand megathrust (Fig. 10A). In addition to the increasing exposure depths and temperatures southward along the proto–Kern Canyon fault (Figs. 2B and 5), the fault also exhibits southward-increasing reverse to thrust components of shear as it flattened southward into the Rand megathrust (Wood, 1997; Saleeby, 2003; Nadin and Saleeby, 2008). These observations are consistent with the hypothesis that the proto–Kern Canyon fault is restricted to the southernmost part of the batholith, in that the north-dipping lateral ramp, as seismically imaged, projects to Moho depths at the same approximate latitude that the southward increase in exposure depth starts (Malin et al., 1995; Nadin and Saleeby, 2008). Rand thrusting is constrained to between 98 and 90 Ma (Saleeby et al., 2007; Chapman et al., 2012), largely overlapping deformation ages of the proto–Kern Canyon fault. In summary, where the broad northern shoulder of the rise conjugate subducted, normal shortening strains were localized at strong thermal contrasts within the central SNB. In contrast, where the massive Tamu conjugate subducted, the entire mantle wedge was sheared off and the shallow Rand subduction megathrust formed.

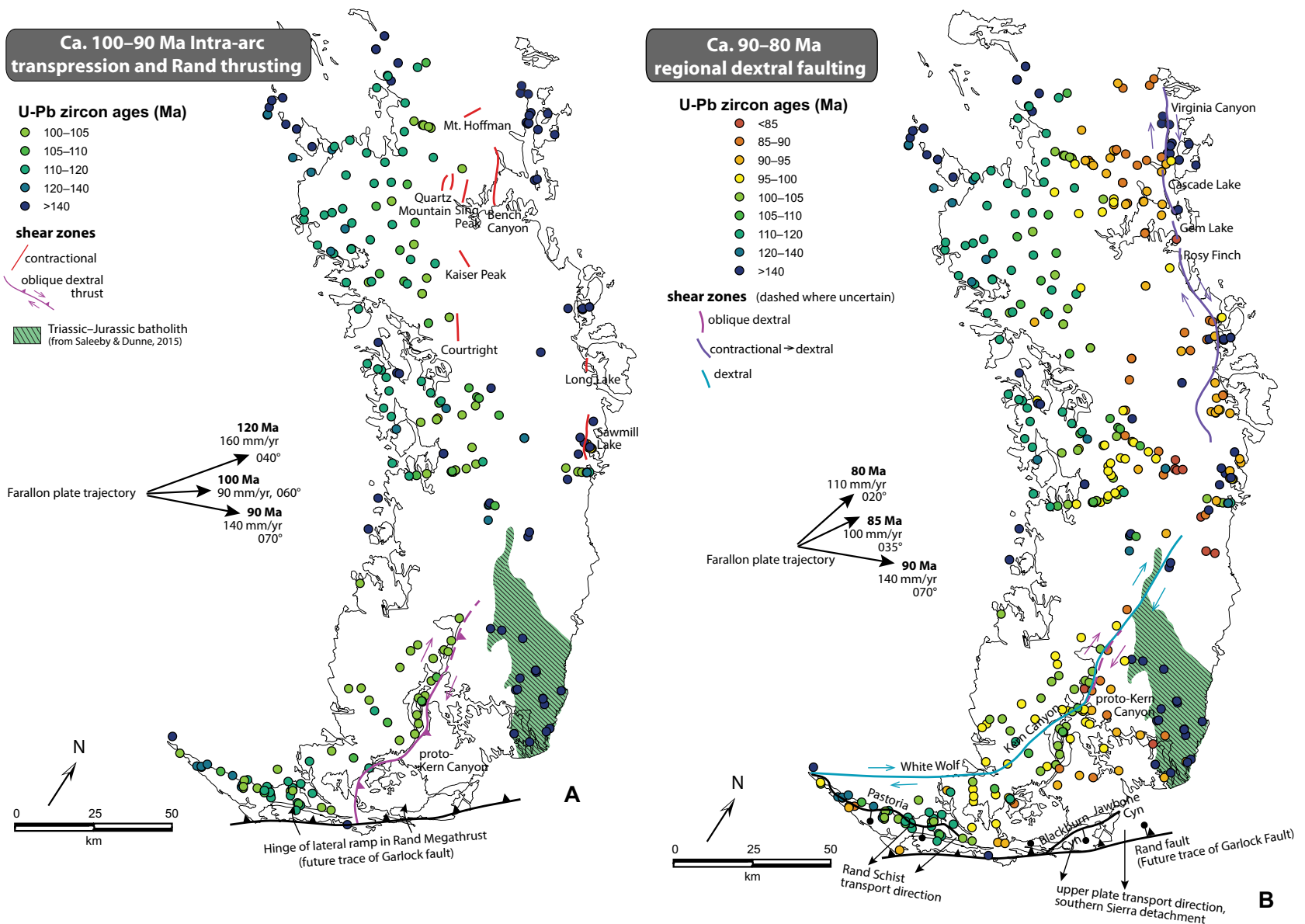


Figure 10. Maps of the general setting of the Sierra Nevada batholith (SNB). (A) During the 100–90 Ma time frame. (B) During the 90–80 Ma time frame. Farallon plate trajectory vectors are adjusted from Figure 9 to reflect the N30W orientation of the SNB, and show convergence directions that are compatible with compression (A) versus dextral shear (B). U-Pb zircon ages (colored dots) are shown to approximate the extent of plutonic rocks present for each time frame. The shear zones that arose from 100 to 90 Ma are relatively short structures dispersed through the central part of the SNB. In contrast, dextral shear zones of the 90–80 Ma central SNB occur at the boundaries between old, cold and young, hot plutons. The shear zones of the southern SNB do not link to those in the north, and were perhaps prevented from doing so by the large swath of Triassic–Jurassic plutons, which is minimally offset by the Kern Canyon fault.

The deformational gradient between these two regions is marked by the profound southward exhumation gradient in the southernmost SNB, and the oblique dextral convergence zone of the proto-Kern Canyon fault. Deep exhumation south of Lake Isabella is likely connected to the multiple ~50-km-length-scale detached upper crustal sheets, which have been identified along the Garlock fault (Fig. 1) and in the San Andreas fault–displaced Salinina terrane of coastal central California (Chapman et al., 2012; Hall and Saleeby, 2013).

Each of these tectonic events contributed to regional and local cooling and deformation within the batholith.

### Origin of the Kern Canyon Fault

The Kern Canyon fault is a Cretaceous ductile to brittle shear zone whose northern trace overprints the northern proto-Kern Canyon fault, and whose southern trace continues southwestward as the White Wolf fault basement damage zone (Fig. 1; e.g., Nadin and Saleeby, 2008, 2010, and references therein). Timing and kinematics distinguish the Kern Canyon–White Wolf from the proto-Kern Canyon zones (Fig. 10; Nadin and Saleeby, 2008, 2010; Saleeby et al., 2009; Chapman et al., 2012).

The thermal history of the Kern Canyon–White Wolf fault zone is difficult to interpret because of a paucity of biotite Ar data along the zone (Fig. 4B), and due to the strong exhumation gradient that developed rapidly along its southeastern wall during its dextral displacement phase (Figs. 2B and 5). In the ca. 85 Ma time frame, the Kern Canyon–White Wolf zone appears to have more strongly controlled the rapid cooling pattern of the southeast Isabella domain than did the proto-Kern Canyon fault. The fact that (U-Th)/He zircon ages from the southeast Isabella domain are virtually identical to biotite Ar ages, within uncertainty (Chapman et al., 2012, fig. 9 therein), attests to rapid cooling (inferred exhumation) in the 86–80 Ma interval. Dextral slip along the Kern Canyon fault and its southwestward continuation into the White Wolf zone (Fig. 1) began ca. 85 Ma. Displacement decreases from as much as 25–30 km of separation in the south, where the zone descends into the southernmost Great Valley subsurface (Ross, 1986; Nadin and Saleeby, 2008; Saleeby et al., 2010), to zero in the north near the Mount Whitney region. In addition, multiple east-west-oriented normal faults are between the Kern Canyon–White Wolf zone and the southeastern margin of the SNB. The thermochronological and structural signatures suggest that Kern Canyon–White Wolf dextral displacement was contemporaneous with large-magnitude north-south extension southeast of the Kern Canyon fault (Wood and Saleeby, 1997; Saleeby et al., 2010; Chapman et al., 2012). Crustal-scale stretching is attributed to coupling across the Rand fault as the Rand Schist was extruded southwestward out of the shallow, low-dipping subduction zone ca. 85 Ma (Saleeby, 2003; Saleeby et al., 2007; Chapman et al., 2010, 2012). This was accompanied by tectonic removal of large overlying upper crustal detachment sheets. The Kern Canyon–White Wolf fault zone partitioned the highly extending southeast Isabella

domain from modest to nonextending Sierran basement to the northwest (Saleeby et al., 2007, 2010; Nadin and Saleeby, 2008; Chapman et al., 2010). Bartley et al. (2007) ascribed ~50 km of Late Cretaceous dextral offset of the SNB along the Owens–Indian Wells Valley region to rapid tectonic exhumation of the southern SNB and to the dextral offset history of the Kern Canyon system. We find merit in this proposition, but point out that the correlative Kern Canyon structure to this regime is the Kern Canyon–White Wolf zone, and not the proto-Kern Canyon zone, as Bartley et al. (2007) stated.

Extrusion of the Rand Schist and coupled overlying large-magnitude extension of the southernmost Sierra have been attributed to (1) gravitational collapse in concert with crustal shortening and surface uplift (Malin et al., 1995; Chapman et al., 2012), and/or (2) focused slab rollback as the trailing edge of the Shatsky Rise conjugate progressed down the subduction zone (Saleeby, 2003). These more localized dynamic effects as the principal drivers for Kern Canyon–White Wolf dextral displacements are in contrast to the plate kinematic mechanism of dextral-sense oblique subduction hypothesized for the northeastern Sierra Crest dextral shear zones (Tobisch et al., 1989, 1993, 1995; Cao et al., 2015; Tikoff and Greene, 1994; Tikoff et al., 2005). The timing for the transition between normal shortening and dextral shear in the central SNB in general reflects the Seton et al. (2012) plate kinematic reconstruction for an abrupt change from effectively normal to dextral convergence ca. 85 Ma (Figs. 9 and 10). We note, however, that the Gem Lake and Rosy Finch dextral shear zones appear to have initiated before the time that the plate kinematic model predicts. One possibility is that the impact of the Shatsky Rise conjugate to the south drove components of dextral shear along the Sierra crest thermal contrast zone, between large Late Cretaceous plutons and significantly older plutons to the east. The significant mass of cooled early Mesozoic plutons in the northeast Isabella domain may have, in this regard, helped transmit impactor tangential stresses northward into the central SNB crest region prior to the ca. 85 Ma change in Farallon plate motions. This mechanism would fail to drive the ca. 85–80 Ma phase of Sierra Crest dextral shear, because the Rand Schist was in its southwestward extrusion phase during that time, indicating that the positively buoyant impactor had progressed down the subduction channel and likely was converting to eclogite (Liu et al., 2010).

The apparent conundrum outlined above for the driver of ca. 85 Ma regional dextral shear may be resolved by the temporal relations of schist extrusion. Geospeedometry based on garnet zonation and textural patterns in the Rand Schist (Chapman et al., 2011), and on thermal evolution patterns along the Rand fault (Saleeby et al., 2007), permit 100-km-scale southwestward extrusion of the schist over very short (~1 m.y.) time scales ca. 85 Ma. Perhaps the entire dextral displacement history of the Kern Canyon–White Wolf zone was compressed into this short time frame, driven by these local dynamic processes, during and after which Farallon plate kinematics propelled the principal dextral displacements of the Sierra Crest shear zone system (Tobisch et al., 1989, 1993, 1995; Cao et al., 2015; Tikoff and Greene, 1994; Tikoff et al., 2005).

## CONCLUSIONS

In this study we map U-Pb zircon (~900 °C), hornblende Ar (~525 °C), and biotite Ar (~325 °C) ages throughout the SNB in order to explore the regional pattern of cooling through brittle-plastic transition temperatures and place localization of shear zones into a thermotectonic context. We report new <sup>40</sup>Ar/<sup>39</sup>Ar biotite, hornblende, muscovite, and K-spar ages, as well as a variety of thermometric determinations, from the proto-Kern Canyon and overprinting Kern Canyon faults in the southern SNB. We contrast intrabatholithic conditions that yielded contractional and transpressional structures, and compare conditions under which shear zones of the central versus southern SNB arose.

Color contour maps of the thermochronometric data reveal a general trend of eastward-younging plutonism punctuated by local thermal anomalies and deformation zones. Contractional deformation ca. 100–90 Ma is recorded along short (<10 km long) shear zones dispersed through the axial zone of the central SNB. In contrast, ca. 90–80 Ma transpressional zones of the Sierra Crest shear zone system are found at the boundary between some of the oldest (older than 140 Ma) and youngest (85–80 Ma) intrusives of the batholith. The thermotemporal juxtaposition of cold, older than 100 Ma and warm, 85–80 Ma rocks of the batholith may have served to localize shear as the central part of the batholith transitioned from contractional to transpressional deformation fields during plate kinematic reconfiguring.

Shear zones of the southern SNB arose under conditions quite different from those to the north, and are separated from them by two distinct thermal barriers: the young, warm Mount Whitney Intrusive Suite and an east-west-oriented corridor of cool rocks just north of lat 36°N, coinciding with a Triassic–Jurassic zone of the batholith. We suggest that these thermal and/or physical perturbations prevented the Sierra Crest shear zone system from propagating southward. The proto-Kern Canyon fault, which was continuously active from ca. 95 to 86 Ma, arose due to local effects of oceanic plateau subduction. Southward-increasing deformation temperatures along the fault track with increasing depths of crystallization for the southernmost SNB and reflect rapid exhumation in the region during and immediately following proto-Kern Canyon fault displacement. The proto-Kern Canyon fault shallows in dip southward and merges with high-grade tectonites of the proximal upper plate of the Rand subduction megathrust. This, in conjunction with the synchronicity of motion of these two regional structures, leads us to interpret the proto-Kern Canyon fault as a whole-crust–penetrating lateral ramp that originated in the southeast part of the batholith and climbed northward out of the Rand megathrust. This lateral ramp nucleated at a major northward inflection in the Farallon plate as it subducted, and we relate this to primary bathymetric structure of the subducted oceanic plateau.

The Kern Canyon–White Wolf fault system overprints the proto-Kern Canyon fault along its northern extent. It initiated in the most deeply exhumed parts of the southwestern SNB, contemporaneous with reversal of Rand fault motion and extrusion of the subducted Rand Schist accretionary assemblage. Its dextral offset diminishes northward, terminating near the youngest and

southernmost pulse of plutonism, the ca. 85 Ma large-volume Mount Whitney Intrusive Suite. In this capacity the Kern Canyon–White Wolf fault system was intimately related to large-magnitude extension of the region, partitioning highly extended basement to the southeast from modestly extended basement to the northwest. The kinematic pattern of large-magnitude extension and dextral displacement along the Kern Canyon–White Wolf system coincides with the extrusion direction of the Rand Schist, and suggests that middle to upper crustal extension was mechanically coupled to lower crustal schist extrusion.

The map patterns of central SNB shear zones are in stark contrast to those of the Kern Canyon–White Wolf system of the southern SNB, including orientation, aerial extent, and overall kinematic patterns (Figs. 1 and 10). We assert that these differences result from different tectonic driving regimes, with the central SNB zones arising from Farallon plate kinematic patterns, and the southern SNB zones arising from more localized dynamic effects of oceanic plateau subduction.

## ACKNOWLEDGMENTS

We thank the many people who have provided assistance through the data collection required for this work. Greg Hirth motivated the study of deformation temperatures along a ductile shear zone. Nobu Shimizu graciously provided assistance in using the Woods Hole Oceanographic Institution ion probe, and in deciphering results. Bill Collins and Joe Devine at Brown University were instrumental in helping to make thin sections and run the electron microprobe, and Ken Severin and Karen Spaleta at University of Alaska Fairbanks enthusiastically figured out how to make TitaniQ work on the AIL probe. Artur Benisek volunteered to determine two-feldspar temperatures from our analyses. Conversations on Sierra Nevada shear zones with many people, notably Basil Tikoff, have helped to steer our thinking. Maria Seton provided the data for the Farallon–North America reconstruction. We thank Phil Gans for <sup>40</sup>Ar/<sup>39</sup>Ar analyses on samples from the Lake Isabella region. Comments by Alan Chapman and an anonymous reviewer improved the clarity of this manuscript. We especially thank Cathy Busby, Associate Editor of this special issue, who took interest in the subject, put up with continued production delays, and contributed greatly to the improvement of this paper.

## REFERENCES CITED

- Ague, J., 1997, Thermodynamic calculation of emplacement pressures for batholithic rocks, California: Implications for the aluminum-in-hornblende barometer: *Geology*, v. 25, p. 563–566, doi:10.1130/0091-7613(1997)025<0563:TCOEPF>2.3.CO;2.
- Ague, J.J., and Brimhall G.H., 1988, Magmatic arc asymmetry and distribution of anomalous plutonic belts in the batholiths of California: Effects of assimilation, crustal thickness, and depth of crystallization: *Geological Society of America Bulletin*, v. 100, p. 912–927, doi:10.1130/0016-7606(1988)100<0912:MAAADO>2.3.CO;2.
- Anderson, J.L., and Smith, D.R., 1995, The effects of temperature and  $f_{O_2}$  on the Al-in-hornblende barometer: *American Mineralogist*, v. 80, p. 549–559.
- Barth, A.P., Walker, J.D., Wooden, J.L., Riggs, N.R., and Schweickert, R.A., 2011, Birth of the Sierra Nevada magmatic arc: Early Mesozoic plutonism and volcanism in the east-central Sierra Nevada of California: *Geosphere*, v. 7, p. 877–897, doi:10.1130/GES00661.1.
- Bartley, J.M., Glazner, A.F., Coleman, D.S., Kylander-Clark, A.R.C., and Friedrich, A.M., 2007, Large Laramide dextral offset across Owens Valley, California, and its possible relation to tectonic unroofing of the southern Sierra Nevada, in Roeske, S.M., et al., Exhumation associated with continental strike-slip fault systems: *Geological Society of America Special Paper* 434, p. 129–148, doi:10.1130/2007.2434(07).
- Barton, M.D., and Hanson, R.B., 1989, Magmatism and the development of low-pressure metamorphic belts: Implications for the western United States and thermal modeling: *Geological Society of America Bulletin*, v. 101, p. 1051–1065, doi:10.1130/0016-7606(1989)101<1051:MATDOL>2.3.CO;2.

- Bateman, P.C., 1988, Constitution and genesis of the central part of the Sierra Nevada Batholith, California: U.S. Geological Survey Open-File Report 88-382, 284 p.
- Bateman, P.C., 1992, Plutonism in the central part of the Sierra Nevada batholith, California: U.S. Geological Survey Professional Paper 1483, 186 p.
- Bateman, P.C., Busacca, A.J., and Sawka, W.N., 1983, Cretaceous deformation in the western foothills of the Sierra Nevada, California: Geological Society of America Bulletin, v. 94, p. 30–42.
- Behr, W.M., Thomas, J.B., and Hervig, R.L., 2011, Calibrating Ti concentrations in quartz for SIMS determinations using NIST silicate glasses and application to the TitanQ geothermobarometer: American Mineralogist, v. 96, p. 1100–1106, doi:10.2138/am.2011.3702.
- Benisek, A., Kroll, H., and Cemic, L., 2004, New developments in two-feldspar thermometry: American Mineralogist, v. 89, p. 1496–1504, doi:10.2138/am-2004-1018.
- Blundy, J.D., and Holland, T.J.B., 1990, Calcic amphibole equilibria and a new amphibole-plagioclase geothermometer: Contributions to Mineralogy and Petrology, v. 104, p. 208–224.
- Brady, R.J., Ducea, M.N., Kidder, S.B., and Saleeby, J.B., 2006, The distribution of radiogenic heat production as a function of depth in the Sierra Nevada batholith, California: Lithos, v. 86, p. 229–244, doi:10.1016/j.lithos.2005.06.003.
- Bürgmann, R., and Pollard, D.D., 1992, Influence of the state of stress on the brittle-ductile transition in granitic rock: Evidence from fault steps in the Sierra Nevada, California: Geology, v. 20, p. 645–648, doi:10.1130/0091-7613(1992)020<0645:IOTSOS>2.3.CO;2.
- Busby-Spera, C.J., and Saleeby, J.B., 1987, Geologic guide to the Mineral King area, Sequoia National Park, California: Los Angeles, Society of Economic Paleontologists and Mineralogists, Pacific Section, 44 p.
- Busby-Spera, C.J., and Saleeby, J.B., 1990, Intra-arc strike-slip fault exposed at batholithic levels in the southern Sierra Nevada, California: Geology, v. 18, p. 255–259, doi:10.1130/0091-7613(1990)018<0255:IASSFE>2.3.CO;2.
- Cao, W., Paterson, S., Memeti, V., Mundil, R., Anderson, J.L., and Schmid, K., 2015, Tracking paleodeformation fields in the Mesozoic central Sierra Nevada arc: Implications for intra-arc cyclic deformation and arc tempos: Lithosphere, v. 7, p. 296–320, doi:10.1130/L389.1.
- Cecil, M.R., Rothenberg, G.L., Ducea, M.N., Saleeby, J.B., and Gehrels, G.E., 2012, Magmatic growth and batholithic root development in the northern Sierra Nevada, California: Geosphere, v. 8, p. 592–606, doi:10.1130/GES00729.1.
- Chapman, A.D., Kidder, S., Saleeby, J.B., and Ducea, M.N., 2010, Role of extrusion of the Rand and Sierra de Salinas schists in Late Cretaceous extension and rotation of the southern Sierra Nevada and vicinity: Tectonics, v. 29, TC5006, doi:10.1029/2009TC002597.
- Chapman, A.D., Luffi, P.I., Saleeby, J.B., and Petersen, S., 2011, Metamorphic evolution, partial melting and rapid exhumation above an ancient flat slab: insights from the San Emigdio Schist, southern California: Journal of Metamorphic Geology, v. 29, no. 6, p. 601–626.
- Chapman, A.D., Saleeby, J.B., Wood, D.J., Piasecki, A., Kidder, S., Ducea, M.N., and Farley, K.A., 2012, Late Cretaceous gravitational collapse of the southern Sierra Nevada batholith, California: Geosphere, v. 8, p. 314–341, doi:10.1130/GES00740.1.
- Chen, J.H., and Moore, J.G., 1982, Uranium-lead isotopic ages from the Sierra Nevada batholith, California: Journal of Geophysical Research, v. 87, no. B6, p. 4761–4784, doi:10.1029/JB087iB06p04761.
- Chen, J.H., and Tilton, G.R., 1991, Applications of lead and strontium isotopic relationships to the petrogenesis of granitoid rocks, central Sierra Nevada batholith, California: Geological Society of America Bulletin, v. 103, p. 439–447, doi:10.1130/0016-7606(1991)103<0439:AOLASI>2.3.CO;2.
- Cherniak, D.J., and Watson, E.B., 2001, Pb diffusion in zircon: Chemical Geology, v. 172, p. 5–24, doi:10.1016/S0009-2541(00)00233-3.
- Clemons, K.M., and Bartley, J.M., 2008, Field and petrofabric relations of the Long Lake shear zone and the Treasure Lakes phase, Lamarck granodiorite, central Sierra Nevada, California: Geological Society of America Abstracts with Programs, v. 40, no. 1, p. 52.
- Clemens-Knot, D., and Saleeby, J.B., 1999, Impinging ring dike complexes in the Sierra Nevada Batholith, California; roots of the Early Cretaceous volcanic arc: Geological Society of America Bulletin, v. 111, p. 484–496.
- Coleman, D.S., and Glazner, A.F., 1998, The Sierra crest magmatic event: Rapid formation of juvenile crust during the Late Cretaceous in California, in Ernst, W.G., and Nelson, C.A., eds., Integrated Earth and environment evolution of the southwestern United States: Columbia, Maryland, Bellwether Publishing, p. 253–272.
- Coleman, D.S., Gray, W., and Glazner, A.F., 2004, Rethinking the emplacement and evolution of zoned plutons: Geochronologic evidence for incremental assembly of the Tuolumne intrusive suite, California: Geology, v. 32, p. 433, doi:10.1130/G20220.1.
- Davis, J.W., 2010, Thermochronology and cooling histories of plutons: Implications for incremental pluton assembly [Ph.D. thesis]: Chapel Hill, University of North Carolina at Chapel Hill, 132 p.
- Davis, J.W., Coleman, D.S., Gracely, J.T., Gaschnig, R., and Stearns, M., 2012, Magma accumulation rates and thermal histories of plutons of the Sierra Nevada batholith, CA: Contributions to Mineralogy and Petrology, v. 163, p. 449–465, doi:10.1007/s00410-011-0683-7.
- DeCelles, P.G., Ducea, M.N., Kapp, P., and Zandt, G., 2009, Cyclicity in Cordilleran orogenic systems: Nature Geoscience, v. 2, p. 251–257.
- de Silva, S.L., Riggs, N.R., and Barth, A.P., 2015, Quickening the pulse: Fractal tempos in arc magmas: Elements, v. 11, no. 2, p. 113–118.
- Dickinson, W.R., and Snyder, W.S., 1978, Plate tectonics of the Laramide orogeny: Boulder, Colorado, Geological Society of America Memoir 151, p. 355–366.
- Dixon, E.T., 1995, An evaluation of hornblende barometry, Isabella to Tehachapi region, southern Sierra Nevada, California [M.S. thesis]: Ann Arbor, University of Michigan, 150 p.
- du Bray, E.A., and Dellinger, D.A., 1998, Potassium-Argon ages for plutons in the eastern and southern Sierra Nevada batholith, California: U.S. Geological Survey Bulletin 1799, 10 p.
- Ducea, M., 2001, The California arc: Thick granitic batholiths, eclogitic residues, lithospheric-scale thrusting and magmatic flare-ups: GSA Today, v. 11, no. 11, p. 4–10, doi: 10.1130/1052-5173(2001)011<0004:TCATGB>2.0.CO;2.
- Ducea, M.N., and Barton, M.D., 2007, Igniting flare-ups in Cordilleran arcs: Geology, v. 35, no. 11, p. 1047–1050.
- Ducea, M.N., Paterson, S.R., and DeCelles, P.G., 2015, High-volume magmatic events in subduction systems: Elements, v. 11, no. 2, p. 99–104.
- Duffield, W.A., and Dalrymple, G.B., 1990, The Taylor Creek Rhyolite of New Mexico: A rapidly emplaced field of lava domes and flows: Bulletin of Volcanology, v. 52, p. 475–487, doi:10.1007/BF00268927.
- Dumitru, T.A., 1990, Subnormal Cenozoic geothermal gradients in the extinct Sierra Nevada magmatic arc: Consequences of Laramide and post-Laramide shallow-angle subduction: Journal of Geophysical Research, v. 95, no. B4, p. 4925–4941, doi:10.1029/JB095iB04p04925.
- Elkins, L.T., and Grove, T.L., 1990, Ternary feldspar experiments and thermodynamic models: American Mineralogist, v. 75, p. 544–559.
- Engelbreton, D.C., Cox, A., and Gordon, R.G., 1985, Relative motions between oceanic and continental plates in the Pacific Basin: Geological Society of America Special Paper 206, 59 p., doi:10.1130/SPE206.
- Evernden, J.F., and Kistler, R.W., 1970, Chronology of emplacement of Mesozoic batholithic complexes in California and western Nevada: U.S. Geological Survey Professional Paper 623, 42 p.
- Fleck, R.J., Kistler, R.W., and Wooden, J.L., 1996, Geochronologic complexities related to multiple emplacement history of the Tuolumne Intrusive Suite, Yosemite National Park, California: Geological Society of America Abstracts with Program, v. 28, p. 65–66.
- Frost, T.P., and Mattinson, J.M., 1993, Age and tectonic implications of mid-Mesozoic calc-alkalic hornblende rich mafic plutonic rocks of the eastern Sierra Nevada, California: Isochron/West, no. 59, p. 11–16.
- Fuhrman, M.L., and Lindsley, D.H., 1988, Ternary-feldspar modeling and thermometry: American Mineralogist, v. 73, p. 201–215.
- Glazner, A., 1991, Plutonism, oblique subduction, and continental growth: An example from the Mesozoic of California: Geology, v. 19, no. 8, p. 784–786.
- Greene, D.C., and Schweickert, R.A., 1995, The Gem Lake shear zone; Cretaceous dextral transpression in the northern Ritter Range pendant, eastern Sierra Nevada, California: Tectonics, v. 14, p. 945–961, doi:10.1029/95TC01509.
- Hall, C.A., and Saleeby, J.B., 2013, Salinia revisited: A crystalline nappe sequence lying above the Nacimiento fault and dispersed along the San Andreas fault system, central California: International Geology Review, v.55, no. 13, p. 1575–1615.
- Harrison, T.M., Grove, M., Lovera, O.M., and Zeitler, P.K., 2005, Continuous thermal histories from inversion of closure profiles: Reviews in Mineralogy and Geochemistry, v. 58, p. 389–409, doi:10.2138/rmg.2005.58.15.
- Hathaway, G.M., and Reed, W.E., 1994, The Long Lake shear zone: Implications for dextral sense shear zones in the Sierra Nevada batholith, east-central California: Geological Society of America Abstracts with Programs, v. 26, no. 7, p. 385.
- Holland, T., and Blundy, J., 1994, Non-ideal interactions in calcic amphiboles and their bearing on amphibole-plagioclase thermometry: Contributions to Mineralogy and Petrology, v. 116, p. 433–447, doi:10.1007/BF00310910.

- Hutton, D.H.W., and Miller, R.B., 1994, Major dip-slip shear zone associated with emplacement of the Tuolumne Intrusive Suite, central Sierra Nevada batholith: *Geological Society of America Abstracts with Programs*, v. 26, p. A133.
- Johnson, B.L., 2013, Structure, construction, and emplacement of the Yosemite Valley Intrusive Suite and the Yosemite Creek Granodiorite in the central Sierra Nevada batholith [M.S. thesis]: San Jose, California, San Jose State University Paper 4280, 89 p.
- Kohn, M., and Northrup, C., 2009, Taking mylonites' temperatures: *Geology*, v. 37, p. 47–50, doi:10.1130/G25081A.1
- Krueger R.J., 2005, Structural evolution of the Sing Peak pendant: Implications for magma chamber construction and mid-Cretaceous deformation in the central Sierra Nevada, California [M.S. thesis]: Lubbock, Texas Tech University, 108 p.
- Lackey, J.S., Valley, J.W., Chen, J.H., and Stockli, D.F., 2008, Evolving magma systems, crustal recycling, and alteration in the central Sierra Nevada batholith: The oxygen isotope record: *Journal of Petrology*, v. 49, p. 1397–1426, doi:10.1093/ptrology/egn030.
- Liu, L., Spasojevic, S., and Gurnis, M., 2008, Reconstructing Farallon plate subduction beneath North America back to the Late Cretaceous: *Science*, v. 322, p. 934–938.
- Liu, L., Gurnis, M., Seton, M., Saleeby, J., Muller, D., and Jackson, J., 2010, The role of oceanic plateau subduction in the Laramide orogeny: *Nature Geoscience*, v. 3, p. 353–357, doi:10.1038/ngeo829.
- Lovera, O.M., 1992, Computer programs to model  $^{40}\text{Ar}/^{39}\text{Ar}$  diffusion data from multidomain samples: *Computers & Geosciences*, v. 18, p. 789–813, doi:10.1016/0098-3004(92)90025-M.
- Mahan, K.H., Bartley, J.M., Coleman, D.S., Glazner, A.F., and Carl, B.S., 2003, Sheeted intrusion of the synkinematic McDoole pluton, Sierra Nevada, California: *Geological Society of America Bulletin*, v. 115, p. 1570–1582, doi:10.1130/B22083.1.
- Mahéo, G., Saleeby, J., Saleeby, Z., and Farley, K., 2009, Tectonic control on southern Sierra Nevada topography, California: *Tectonics*, v. 28, no. 6, TC6006, doi:10.1029/2008TC002340.
- Malin, P.E., Goodman, E.D., Henyey, T.L., Li, Y.G., Okaya, D.A., and Saleeby, J.B., 1995, Significance of seismic reflections beneath a tilted exposure of deep continental crust, Tehachapi Mountains, California: *Journal of Geophysical Research*, v. 100, p. 2069–2087, doi:10.1029/94JB02127.
- May, J., and Hewitt, R., 1948, The basement complex in well samples from the Sacramento and San Joaquin Valleys, California: *California Journal of Mines and Geology*, v. 44, p. 129–158.
- McDougall, I., and Harrison, T.M., 1999, *Geochronology and thermochronology by the  $^{40}\text{Ar}/^{39}\text{Ar}$  method* (second edition): New York, Oxford University Press, 269 p.
- McNulty, B.A., 1995, Shear zone development during magmatic arc construction: The Bench Canyon shear zone, central Sierra Nevada, California: *Geological Society of America Bulletin*, v. 107, p. 1094–1107, doi:10.1130/0016-7606(1995)107<1094:SZDDMA>2.3.CO;2.
- McNulty, B.A., Tobisch, O.T., Cruden, A.R., and Gilder, S., 2000, Multistage emplacement of the Mount Givens pluton, central Sierra Nevada batholith, California: *Geological Society of America Bulletin*, v. 112, p. 119–135, doi:10.1130/0016-7606(2000)112<119:MEOTMG>2.0.CO;2.
- Nadin, E.S., and Saleeby, J.B., 2008, Disruption of regional primary structure of the Sierra Nevada batholith by the Kern Canyon fault system, California, *in* Wright, J.E., and Shervais, J.W., eds., *Ophiolites, arcs, and batholiths: A tribute to Cliff Hopson*: Geological Society of America Special Paper 438, p. 429–454, doi:10.1130/2008.2438(15).
- Nadin, E.S., and Saleeby, J.B., 2010, Quaternary reactivation of the Kern Canyon fault system, southern Sierra Nevada, California: *Geological Society of America Bulletin*, v. 122, p. 1671–1685.
- Passchier, C.W., and Trouw, R.A.J., 2005, *Microtectonics*: Berlin, Springer Verlag, 366 p., doi:10.1007/3-540-29359-0.
- Paterson, S.R., and Ducea, M.N., 2015, Arc magmatic tempo; gathering the evidence: *Elements*, v. 11, no. 2, p. 91–98.
- Paterson, S., Onezime, J., Teruya, L., and Zak, J., 2003, Quadruple-pronged enclaves: Their significance for the interpretation of multiple magmatic fabrics in plutons: *Journal of the Virtual Explorer*, v. 10, p. 16.
- Paterson, S.R., Okaya, D., Memeti, V., Economos, R., and Miller, R.B., 2011, Magma addition and flux calculations of incrementally constructed magma chambers in continental margin arcs: Combined field, geochronologic, and thermal modeling studies: *Geosphere*, v. 7, p. 1439–1468, doi:10.1130/GES00696.1.
- Peck, D., 1980, Geologic map of the Merced Peak quadrangle, central Sierra Nevada, California: U.S. Geological Survey Geologic Quadrangle Map GQ-1531, scale 1:62,500.
- Pickett, D.A., and Saleeby, J.B., 1993, Thermobarometric constraints on the depth of exposure and conditions of plutonism and metamorphism at deep levels of the Sierra Nevada batholith, Tehachapi Mountains, California: *Journal of Geophysical Research*, v. 98, no. B1, p. 609–629, doi:10.1029/92JB01889.
- Putirka, K.D., 2008, Thermometers and barometers for volcanic systems: Reviews in Mineralogy and Geochemistry, v. 69, p. 61–120, doi:10.2138/rmg.2008.69.3.
- Renne, P.R., Tobisch, O.T., and Saleeby, J.B., 1993, Thermochronologic record of pluton emplacement, deformation and exhumation at Courtright shear zone: *Geology*, v. 21, p. 331–334, doi:10.1130/0091-7613(1993)021<0331:TROPED>2.3.CO;2.
- Richter, F.M., Lovera, O.M., Harrison, T.M., and Copeland, P., 1991, Tibetan tectonics from  $^{40}\text{Ar}/^{39}\text{Ar}$  analysis of a single K-feldspar sample: *Earth and Planetary Science Letters*, v. 105, p. 266–278, doi:10.1016/0012-821X(91)90136-6.
- Ross, D.C., 1986, Basement-rock correlations across the White Wolf–Breckenridge–southern Kern Canyon fault zone, southern Sierra Nevada, California: U.S. Geological Survey Bulletin B1651, 25 p.
- Sager, W.W., 2005, What built Shatsky Rise, a mantle plume or ride tectonics?, *in* Foulger, G.R., et al., eds., *Plates, plumes and paradigms*: Geological Society of America Special Paper 388, p. 721–733, doi:10.1130/2005.2388(41).
- Saleeby J.B., 2003, Segmentation of the Laramide slab—Evidence from the southern Sierra Nevada region: *Geological Society of America Bulletin*, v. 115, p. 655–668, doi:10.1130/0016-7606(2003)115<0655:SOTLSF>2.0.CO;2.
- Saleeby, J., 2007, Western extent of the Sierra Nevada batholith in the Great Valley basement: *Eos (Transactions, American Geophysical Union)*, v. 88, no. 52, p. F2186.
- Saleeby, J., 2014, Southern Cordillera ophiolite associations, northern Cordillera superterrane accretion, and deep mantle seismic wave speed anomalies: An integrated synthesis: *Geological Society of America Abstracts with Programs*, v. 46, no. 6, p. 657.
- Saleeby, J.B., and Busby, C.J., 1993, Paleogeographic and tectonic setting of axial and western metamorphic framework rocks of the southern Sierra Nevada, California, *in* Dunne, G., and McDougall, K., eds., *Mesozoic paleogeography of the western United States—II: Pacific Section, Society for Sedimentary Geology (SEPM) Field Trip Guidebook 71*, p. 197–226.
- Saleeby, J.B., and Busby-Spera, C.J., 1986, Fieldtrip guide to the metamorphic framework rocks of the Lake Isabella area, southern Sierra Nevada, California, *in* Dunne, G.C., ed., *Mesozoic and Cenozoic structural evolution of selected areas, east-central California*: Los Angeles, California, Geological Society of America Cordilleran Section, p. 81–94.
- Saleeby, J., and Dunne, G., 2015, Temporal and tectonic relations of early Mesozoic arc magmatism, southern Sierra Nevada, California, *in* Anderson, T.H., et al., eds., *Late Jurassic margin of Laurasia—A record of faulting accommodating plate rotation*: Geological Society of America Special Paper 513, doi:10.1130/2015.2513(05).
- Saleeby, J.B., Farley, K.A., Kistler, R.W., and Fleck, R., 2007, Thermal evolution and exhumation of deep-level batholithic exposures, southernmost Sierra Nevada, California, *in* Cloos, M., et al., eds., *Convergent margin terranes and associated regions: A tribute to W.G. Ernst*: Geological Society of America Special Paper 419, p. 39–66, doi:10.1130/2007.2419(02).
- Saleeby, J., Ducea, M.N., Busby, C., Nadin, E., and Wetmore, P.H., 2008, Chronology of pluton emplacement and regional deformation in the southern Sierra Nevada batholith, California, *in* Wright, J.E., and Shervais, J.W., eds., *Ophiolites, arcs, and batholiths: A tribute to Cliff Hopson*: Geological Society of America Special Paper 438, p. 397–427, doi:10.1130/2008.2438(14).
- Saleeby, J.B., Saleeby, Z., Nadin, E., and Maheo, G., 2009, Step-over in the structure controlling the regional west tilt of the Sierra Nevada Microplate; eastern escarpment system to Kern Canyon system: *International Geology Review*, v. 51, no. 7–8, p. 634–669.
- Saleeby, J., Saleeby, Z., Liu, L., and Maheo, G., 2010, Mid-Cretaceous regional exhumation of the Sierra Nevada–Great Valley batholith and a possible tectonic driving mechanism: *Geological Society of America Abstracts with Programs*, v. 42, no. 4, p. 67.
- Schmidt, M.W., 1992, Amphibole composition in tonalite as a function of pressure; an experimental calibration of the Al-in-hornblende barometer: *Contributions to Mineralogy and Petrology*, v. 110, p. 304–310, doi:10.1007/BF00310745.
- Segall, P., McKee, E.H., Martel, S.J., and Turrin, B.D., 1990, Late Cretaceous age of fractures in the Sierra Nevada batholith, California: *Geology*, v. 18, p. 1248–1251, doi:10.1130/0091-7613(1990)018<1248:LCAOFL>2.3.CO;2.
- Seton, M., et al., 2012, Global continental and ocean basin reconstructions since 200 Ma: *Earth-Science Reviews*, v. 113, p. 212–270, doi:10.1016/j.earscirev.2012.03.002.
- Sharp, W.D., Tobisch, O.T., and Renne, P.R., 1993, Late Cretaceous (85–90 Ma), syn-arc cleavage development in metamorphic rocks of the Ritter Range, central Sierra Nevada, California: *Geological Society of America Abstracts with Programs*, v. 25, no. 5, p. 145.
- Sharp, W.D., Tobisch, O.T., and Renne, P.R., 2000, Development of Cretaceous transpressional cleavage synchronous with batholith emplacement, central Sierra Nevada, California: *Geo-*

- logical Society of America Bulletin, v. 112, p. 1059–1066, doi:10.1130/0016-7606(2000)112<1059:DOCTCS>2.0.CO;2.
- Stern, T.W., Bateman, P.C., Morgan, B.S., Newell, M.F., and Peck, D.L., 1981, Isotopic U-Pb ages of zircon from the granitoids of the central Sierra Nevada, California: U.S. Geological Survey Professional Paper 1185, 17 p.
- Stöckhert, B., Brix, M.R., Kleinschrodt, R., Hurford, A.J., and Wirth, R., 1999, Thermochronometry and microstructures of quartz—A comparison with experimental flow laws and predictions on the temperature of the brittle-plastic transition: *Journal of Structural Geology*, v. 21, p. 351–369, doi:10.1016/S0191-8141(98)00114-X.
- Thomas, J.B., Watson, E.B., Spear, F.S., Shemella, P.T., Nayak, S.K., and Lanzirotti, A., 2010, TitaniumQ under pressure: The effect of pressure and temperature on the solubility of Ti in quartz: *Contributions to Mineralogy and Petrology*, v. 160, p. 743–759, doi:10.1007/s00410-010-0505-3.
- Tikoff, B., 1994, Transpression: Strain theory and application to the emplacement and deformation of granite, Sierra Nevada, California [Ph.D. thesis]: Minneapolis, University of Minnesota, 277 p.
- Tikoff, B., and de Saint Blanquat, M., 1997, Transpressional shearing and strike-slip partitioning in the Late Cretaceous Sierra Nevada magmatic arc, California: *Tectonics*, v. 16, p. 442–459, doi:10.1029/97TC00720.
- Tikoff, B., and Greene, D.C., 1994, Transpressional deformation within the Sierra Crest shear zone system, Sierra Nevada, California (92–80 Ma): Vertical and horizontal stretching lineations within a single shear zone: *Geological Society of America Abstracts with Programs*, v. 26, no. 7, p. 385.
- Tikoff, B., and Greene, D., 1997, Stretching lineations in transpressional shear zones: An example from the Sierra Nevada Batholith, California: *Journal of Structural Geology*, v. 19, p. 29–39, doi:10.1016/S0191-8141(96)00056-9.
- Tikoff, B., and Teyssier, C., 1992, Crustal-scale, en echelon “P-shear” tensional bridges: A possible solution to the batholithic room problem: *Geology*, v. 20, p. 927–930, doi:10.1130/0091-7613(1992)020<0927:CSEEPS>2.3.CO;2.
- Tikoff, B., Davis, M.R., Teyssier, C., Saint-Blanquat, M., Habert, G., and Morgan, S., 2005, Fabric studies within the Cascade Lake shear zone, Sierra Nevada, California: *Tectonophysics*, v. 400, p. 209–226, doi:10.1016/j.tecto.2005.03.003.
- Tobisch, O.T., Paterson, S.R., and Saleeby, J.B., 1989, Magmatic fabrics in Late Cretaceous granitoids, central Sierra Nevada (CSN), California: Implications for late Mesozoic tectonic models: *Geological Society of America Abstracts with Programs*, v. 21, no. 5, p. 151.
- Tobisch, O.T., Renne, P., and Saleeby, J.B., 1993, Deformation resulting from regional extension during pluton ascent and emplacement, central Sierra Nevada, California: *Journal of Structural Geology*, v. 15, p. 609–628, doi:10.1016/0191-8141(93)90151-Y.
- Tobisch, O.T., Saleeby, J.B., Renne, P.R., McNulty, B., and Tong, W.X., 1995, Variations in deformation fields during development of a large-volume magmatic arc, central Sierra Nevada, California: *Geological Society of America Bulletin*, v. 107, p. 148–166, doi:10.1130/0016-7606(1995)107<0148:VIDFDD>2.3.CO;2.
- Tong, W., 1994, Nature, physical conditions and time constraints of ductile deformation and pluton emplacement in the Quartz Mountain area, Sierra Nevada, California and within the Changle-Nanao shear zone, Dongshan area, southeast China [Ph.D. thesis]: Santa Cruz, University of California–Santa Cruz, 182 p.
- Wark, D.A., and Watson, E.B., 2006, TitaniumQ: A titanium-in-quartz geothermometer: *Contributions to Mineralogy and Petrology*, v. 152, p. 743–754, doi:10.1007/s00410-006-0132-1.
- Wen, S., and Nekvasil, H., 1994, SOLVCALC: An interactive graphics program package for calculating the ternary feldspar solvus and for two-feldspar geothermometry: *Computers & Geosciences*, v. 20, p. 1025–1040, doi:10.1016/0098-3004(94)90039-6.
- Wood, D.J., 1997, Geology of the eastern Tehachapi Mountains and Late Cretaceous–early Cenozoic tectonics of the southern Sierra Nevada region, Kern County, California [Ph.D. thesis]: Pasadena, California Institute of Technology, 287 p.
- Wood, D.J., and Saleeby, J.B., 1997, Late Cretaceous–Paleocene extensional collapse and disaggregation of the southernmost Sierra Nevada batholith: *International Geology Review*, v. 39, p. 973–1009, doi:10.1080/00206819709465314.